Molecular Biology of the Cell
Vol. 20, 1102–1117, February 1, 2009

Zona Occludens-2 Inhibits Cyclin D1 Expression and Cell Proliferation and Exhibits Changes in Localization along the Cell Cycle

Rocio Tapia,* Miriam Huerta,† Socorro Islas,* Antonia Avila-Flores,‡ Esther Lopez-Bayghen,† Jörg Weiske,§ Otmar Huber,§‖ and Lorenza González-Mariscal*

*Department of Physiology, Biophysics, and Neuroscience, and †Department of Genetics and Molecular Biology, Center for Research and Advanced Studies (CINVESTAV), Mexico, D.F., 07360, Mexico; ‡Department of Immunology and Oncology, National Center for Biotechnology, Consejo Superior de Investigaciones Cientificas, Campus Cantoblanco, E-28049 Madrid, Spain; §Department of Laboratory Medicine and Pathobiochemistry, Charité-Universitätsmedizin Berlin, 12200 Berlin, Germany; and ‖Department of Biochemistry II, Friedrich-Schiller-University Jena, 07743 Jena, Germany

Submitted March 14, 2008; Revised October 28, 2008; Accepted November 21, 2008
Monitoring Editor: Keith E. Mostov

Here, we have studied the effect of the tight junction protein zona occludens (ZO)-2 on cyclin D1 (CD1) protein expression. CD1 is essential for cell progression through the G1 phase of the cell cycle. We have found that in cultures of synchronized Madin-Darby canine kidney cells, ZO-2 inhibits cell proliferation at G0/G1 and decreases CD1 protein level. These effects occur in response to a diminished CD1 translation and an augmented CD1 degradation at the proteosome triggered by ZO-2. ZO-2 overexpression decreases the amount of Glycogen synthase kinase-3β phosphorylated at Ser9 and represses β-catenin target gene expression. We have also explored the expression of ZO-2 through the cell cycle and demonstrate that ZO-2 enters the nucleus at the late G1 phase and leaves the nucleus when the cell is in mitosis. These results thus explain why in confluent quiescent epithelia ZO-2 is absent from the nucleus and localizes at the cellular borders, whereas in sparse proliferating cultures ZO-2 is conspicuously present at the nucleus.

INTRODUCTION

Epithelial sheets constitute the frontier between the external environment and the internal milieu in multicellular organisms. Epithelial cells attach to each other by a group of intercellular contacts. At the uppermost portion of the lateral membrane, the paracellular space is sealed by tight junctions (TJs). This structure performs two crucial functions in epithelial cells: it both regulates the transit of ions and molecules via the intercellular space and maintains a polarized distribution of lipids and proteins between the apical and basolateral domains, by blocking their free diffusion within the plasma membrane.

The TJ is constituted by transmembrane and adaptor proteins. Although the former establish cell–cell contact through their extracellular domains, the latter work as scaffolds that reunite at a specific region of the membrane, a complex set of proteins that includes kinases, phosphatases, transcription factors (TFs), and small guanosine triphosphate-binding proteins, among others (for a review on TJ proteins, see Gonzalez-Mariscal *et al*., 2003).

This article was published online ahead of print in *MBC in Press* (http://www.molbiolcell.org/cgi/doi/10.1091/mbc.E08–03–0277) on December 3, 2008.

Address correspondence to: Lorenza Gonzalez-Mariscal (lorenza@fisio.cinvestav.mx).

ZO-2 is a member of the *m*embrane *a*ssociated *gu*anylate *k*inase homologous protein family (MAGUK) (Gumbiner *et al*., 1991). All identified family members include characteristic postsynaptic density 95/disc-large/zona occludens (PDZ), Src homology 3 (SH3) and guanylate kinase-like (GK) domains, all of them known to be involved in protein–protein interactions (Gonzalez-Mariscal *et al*., 2000).

Junctional proteins not only exert functions related to their barrier role at the plasma membrane but also are involved in signal transduction, transferring information to the cell interior to modulate cell proliferation and differentiation (Balda *et al*., 2003; Sourisseau *et al*., 2006). First evidence that this role may be attributed to ZO proteins was given from their high homology to the tumor suppressor protein DlgA (Willott *et al*., 1993; Woods *et al*., 1997). This notion has been further supported by the observation that in several carcinomas the expression of junctional proteins is down-regulated (for review, see Gonzalez-Mariscal *et al*., 2007) as shown for ZO-2 in breast and pancreatic cancer (Chlenski *et al*., 1999, 2000).

Furthermore, ZO-2 has been found to be a target for viral oncoproteins. Hence, the transforming potential of the adenovirus type 9 oncogenic determinant E4 (Ad9 E4-ORF1) is associated with its ability to bind and aberrantly sequester ZO-2 within the cytoplasm, whereas the overexpression of ZO-2 inhibits Ad9 E4-ORF1–induced transformation (Glaunsinger *et al*., 2001; Latorre *et al*., 2005).

The subcellular distribution of ZO-2 is responsive to the degree of cell–cell contact. Thus in confluent epithelial

monolayers, ZO-2 localizes at the TJ, whereas in sparse cultures characterized for their high proliferative state, a significant amount of ZO-2 concentrates in the nucleus (Islas *et al*., 2002). There, ZO-2 associates to the nuclear matrix (Jaramillo *et al*., 2004), displays a speckled distribution, and colocalizes with the essential splicing factor SC-35 (Islas *et al*., 2002), and with the nuclear scaffold attachment factor SAF-B (Traweger *et al*., 2003), a corepressor of estrogen receptor-α known to regulate the transcription of genes involved in proliferation, apoptosis, and migration. For its movement in and out of the nucleus, four nuclear localization and five export signals have been identified previously (Islas *et al*., 2002; Jaramillo *et al*., 2004; Gonzalez-Mariscal *et al*., 2006).

In a previous work, we demonstrated the specific interaction of ZO-2 with Jun and Fos TFs, which form a transcription complex named AP-1 (Betanzos *et al*., 2004). Because AP-1 is involved in cell proliferation, transformation, and death (Shaulian and Karin, 2002), we explored the impact of ZO-2 expression on the activity of the CD1 promoter, and observed that ZO-2 down-regulates CD1 transcription by interacting with the c-Myc/E box element and by recruiting histone deacetylases (Huerta *et al*., 2007).

CD1 is rate limiting and essential for cell progression through the G1 phase of the cell cycle. CD1 binds to and activates the cyclin-dependent kinases Cdk4 and Cdk6, which in turn phosphorylate their downstream target the retinoblastoma protein (Rb). The latter binds to and negatively regulates the activities of E2F TFs. On Rb-dependent phosphorylation, E2F TFs are liberated and hence activate the expression of the S phase genes, thereby inducing cell cycle progression (Coqueret, 2002).

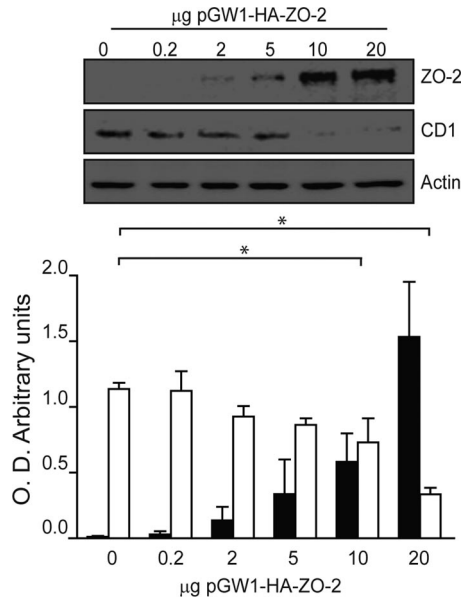

Figure 1. Transfected ZO-2 diminishes in a dose-dependent manner the amount of CD1 protein in sparse MDCK cultures. One day after plating at a sparse condition, MDCK cultures were transfected with increasing amounts of pGW1-HA-ZO-2. Forty-eight hours, later the monolayers were lysed, subjected to SDS-PAGE, and the proteins were blotted with antibodies against ZO-2, CD1, and actin. In this figure as in Figures 7–9, the blot illustrates one representative example, and the graph shows the densitometric analysis of at least three independent experiments. Full bars correspond to ZO-2/actin, and empty bars correspond to CD1/actin. (*$p \leq 0.001$, according to ANOVA Tukey's multiple comparison test).

Here, we have analyzed the impact of ZO-2 overexpression on epithelial cell proliferation and CD1 expression. Our results indicate that ZO-2 overexpression inhibits cell proliferation by blocking progression of cells through the cell cycle at the G1/S boundary. ZO-2 decreases CD1 protein levels by diminishing its translation and increasing its degradation at the proteosome. In addition, we observed that the nuclear expression of ZO-2 varies with the cell cycle as ZO-2 enters the nucleus at the late stage of G1 and leaves the nucleus during mitosis.

MATERIALS AND METHODS

Cell Culture

Epithelial Madin-Darby canine kidney (MDCK) cells between the 60th and 90th passage were grown as described previously (Gonzalez-Mariscal *et al*., 1985). Cells were harvested with trypsin-EDTA and plated either sparse (1×10^5 cells/cm^2) or at confluence (3×10^5 cells/cm^2). The synchronized cultures in the sparse condition cells were plated at an initial density of 0.5×10^5 cells/cm^2. Human embryonic kidney (HEK) 293, SW480, and MCF-7 cells were cultured as described previously (Weiske and Huber, 2006).

Expression Plasmids, Small Interfering RNAs (siRNAs), and Transfection Assays

Full-length canine ZO-2 introduced into the cytomegalovirus expression plasmid pGW1 (pGW1-HA-ZO-2) was kindly provided by Ronald Javier (Baylor

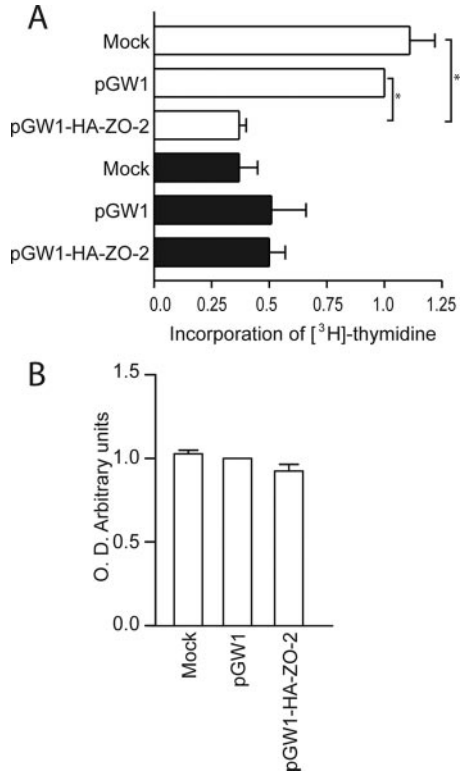

Figure 2. ZO-2 overexpression inhibits [^{3}H]thymidine incorporation into sparse MDCK cells without inducing cell death. (A) DNA synthesis was determined by the incorporation of [^{3}H]thymidine in sparse (empty bars) and confluent (full bars) cultures of MDCK cells synchronized by incubation for 48 h with media with 0.1% serum. For normalization, we gave a value of 1 to the counts obtained in the sparse cells transfected with the empty vector. Results are reported as mean values ± SE, from four independent experiments. (*$p \leq 0.001$, according to ANOVA Tukey's multiple comparison test). (B) Synchronized cultures of sparse MDCK cells were transfected with the empty vector or pGW1-HA-ZO-2. After 24 h, cells were harvested, and viable cells were counted by trypan blue exclusion.

College of Medicine, Houston, TX). The amino-terminal (NH_2, containing PDZ1, PDZ2, and PDZ3 domains; 398-2165 nucleotides [nt]), middle (3PSG, containing PDZ3, SH3, and GuK domains; 1595–3019 nt), and carboxy-terminal (AP, containing the acidic and proline-rich regions; 3029–3923 nt) segments of canine ZO-2 were introduced into pcDNA4/HisMax as reported previously (Betanzos *et al*., 2004; Jaramillo *et al*., 2004). pCB6-ZO-1myc was kindly provided by Dr. Maria Susana Balda (Institute of Ophthalmology, University College of London, London, United Kingdom).

Wnt reporter gene assays were performed as described previously (Weiske *et al*., 2007). HEK293 cells (5×10^5) were transfected with the calcium-phosphate method. The following amounts of expression vectors were used for transfections: 1.0 μg of the Siamois-luciferase (S5, S0) or Topflash/Fopflash (pGL3-OT/OF) reporter constructs (kindly provided by David Kimelman [University of Washington, Seattle, WA] and Bert Vogelstein [Johns Hopkins University School of Medicine, Baltimore, MD], respectively), 0.75 μg of hTCF4 (kindly provided by Hans Clevers [Hubrecht Institute for Developmental Biology and Stem Cell Research, Utrecht, The Netherlands]), and 0.75 μg of β-catenin expression vectors. To normalize transfection efficiency 0.1 μg pHRL-TK (*Renilla* luciferase) (Promega, Madison, WI) was cotransfected. The amount of DNA for each transfection was adjusted by addition of empty pCS2+ vector. Reporter gene assays were performed with the Dual-Luciferase Reporter Assay System (Promega). Luciferase activity was measured 42 h after transfection in a Lumat LB9507 luminometer (Berthold Technologies, Bad Wildbad, Germany). Mean values of four independent transfection experiments measured in duplicate are presented for all reporter gene assays.

The Stealth siRNA for ZO-2 was described previously (Hernandez *et al*., 2007). The siRNA-negative control NC was obtained from Invitrogen (Carlsbad, CA) and is not homologous to any sequence in vertebrate transcriptomes. Transfections were performed with Lipofectamine 2000 (Invitrogen) as indicated by the manufacturer.

Drugs

Nocodazole (Sigma-Aldrich, St. Louis, MO) was prepared as a 0.55 μg/μl stock in dimethyl sulfoxide (DMSO) and added to DMEM to a final concentration of 0.1 μg/ml. Cloroquine (Sigma-Aldrich) was prepared as a 10 mM stock in DMSO and added to DMEM to a final concentration of 100 μM. MG132 (Sigma-Aldrich) was prepared as a 20 mM stock in DMSO and added to DMEM to a final concentration of 50 μM. Staurosporine (Calbiochem, Darmstadt, Germany) was prepared as a 214 μM stock in DMSO and added to DMEM to a final concentration of 0.5 or 1.0 μM. Rapamycin (Calbiochem, Darmstadt, Germany) was prepared as a 0.01 μg/μl stock in DMSO and added to DMEM to a final concentration of 20 nM. The highest DMSO final concentration in medium (0.01%) had no effect in control experiments.

L-Mimosine (Sigma-Aldrich) was prepared at a concentration of 1 mM in DMEM. LiCl (Mallinckrodt, St. Louis, MO) was prepared as a 1 M stock in phosphate-buffered saline (PBS) and added to DMEM to a final concentration of 50 mM. Cycloheximide (Sigma-Aldrich) was prepared as a 1 mg/ml stock in PBS and added to DMEM to a final concentration of 50 μg/ml.

Cellular Lysates and Protein Blotting

For the Western blot detection of ZO-2, CD1, actin, GSK-3β, and phosphorylated Ser9 of GSK-3β, MDCK cells were lysed under gentle rotation for 15 min at 4°C with radioimmunoprecipitation assay buffer [40 mM Tris-HCl, pH 7.6, 150 mM NaCl, 2 mM EDTA pH 8.0, 10% (vol/vol) glycerol, 1% (vol/vol) Triton X-100, 0.5% (wt/vol) sodium deoxycholate, 0.2% (wt/vol) SDS, and 1 mM phenylmethylsulfonyl fluoride [PMSF]) containing the protease inhibitor cocktail Complete (Roche Diagnostics, Mannheim, Germany). For the Western blot detection of *m*ammalian *t*arget *o*f *r*apamycin (mTOR), phosphorylated Ser2448 and Ser2481 of mTOR, of p70 S6K and phosphorylated Thr389 and Thr421/Ser424 of p70 S6K and 4E-BP1, the cells were lysed under gentle rotation for 15 min at 4°C in p70 buffer [10 mM HEPES, pH 7.5, 15 mM KCl, 1 mM EDTA, 1 mM EGTA, 10% (vol/vol) glycerol, 0.2% (vol/vol) NP-40, 1 mM dithiothreitol, 50 mM NaF, 10 μg/ml leupeptin and aprotinin, 1 mM PMSF, 1 mM sodium orthovanadate, and 20 mM β-glycerol phosphate).

Subsequently the lysates were sonicated three times for 30 s each in a high intensity ultrasonic processor (Vibra cell, Sonics and Materials, Danbury, CT). The proteins in the cellular extracts were quantified and the samples were diluted (1:1) in sample buffer (125 mM Tris-HCl, 4% (wt/vol) SDS, 20% (vol/vol) glycerol, 10% (vol/vol) 2-mercaptoethanol, pH 6.8), run in 12% polyacrylamide gels, and transferred to polyvinylidene difluoride membranes (GE Healthcare, Little Chalfont, Buckinghamshire, United Kingdom).

Blotting was performed with polyclonal antibodies against ZO-2 (catalog no. 71-1400, dilution 1:1000; Zymed Laboratories, South San Francisco, CA.), CD1 (catalog no. sc-717, dilution 1:1000; Santa Cruz Biotechnology, Santa Cruz, CA), phosphorylated Ser2448 of mTOR (catalog no. 2971, dilution 1:1000; Cell Signaling Technology, Danvers, MA.), phosphorylated Ser2481 of mTOR (catalog no. 2974, dilution 1:1000; Cell Signaling Technology, Danvers, MA.), mTOR (catalog no. 2983, dilution 1:1000; Cell Signaling Technology.); 4E-BP1 (catalog no. 9452, dilution 1:1000, Cell Signaling Technology), phosphorylated Thr389 of p70 S6K (catalog no. 9205, dilution 1:1000; Cell Signaling Technology), phosphorylated Thr421/Ser424 of p70 S6K (catalog no. 9204, dilution 1:1000; Cell Signaling Technology), p70 S6K (catalog no. 9202, dilution 1:1000; Cell Signaling Technology), phosphorylated Ser9 of GSK-3β (catalog no. 9336, dilution 1:1000; Cell Signaling Technology) or with monoclonals against GSK-3β (catalog no. G22320, dilution 1:1000; BD Biosciences Transduction Laboratories, Lexington, KY) or against actin, generated and generously provided by Dr. José Manuel Hernandez (Department of Cell Biology, CINVESTAV, Mexico) (dilution 1:50). Peroxidase-conjugated goat immunoglobulin G (IgG) against rabbit IgG or against mouse IgG (catalog nos. 62–6120 and 62–6520, respectively; dilution 1:3000; Zymed Laboratories, South San Francisco, CA) were used as secondary antibodies, followed by ECL+Plus chemiluminescence detection (GE Healthcare).

Synchronization of Cell Cultures and Cell Cycle Analysis with Propidium Iodide

MDCK cells were plated at confluent or sparse density in DMEM (D1152; Sigma-Aldrich) with penicillin (100 IU/ml; Eli Lilly, Mexico City, Mexico) and 10% (vol/vol) iron supplemented certified calf serum (10371-029; Invitrogen). After 24 h, the cells were transferred to DMEM containing 0.1% (vol/vol) of serum for 48 h (condition A in Figures 3 and 6). Cell cycle entry was then triggered by addition of 10% (vol/vol) serum (CDMEM) for 24 h (condition B in Figure 3). Next, a group of cells was transfected with pGW1-HA-ZO-2 or the empty vector and analyzed 24 h later (condition C in Figures 3 and 6). Alternatively, 48 h after serum starvation, the cells were transfected with pGW1-HA-ZO-2, His/Max-NH_2-ZO-2, His/Max-3PSG-ZO-2, His/Max-AP-ZO-2 or the corresponding empty vectors, and 6 h after transfection transferred to CDMEM. Then, 24 h later the cells were analyzed (condition D in Figures 3 and 6). In yet another experiment, the sparse and unsynchronized cells were transfected with pGW1-HA-ZO-2 or the empty vector, and 6 h after transfection they were submitted to serum deprivation [0.1% (vol/vol) serum] for 48 h (condition E in Figure 6).

For the determination of the percentage of cells present in each phase of the cell cycle a standard procedure was followed (Dasso, 1999). Briefly, the cells were trypsinized, fixed, and permeabilized in 70% (vol/vol) ice-cold ethanol to make them accessible to propidium iodide (PI). Once fixed, the cells were rinsed with PBS and stained with a PBS solution containing 0.1% (vol/vol) Triton X-100, 0.20 mg/ml DNase-free RNase A, and 0.02 mg/ml PI. Triton X-100 was included to decrease the cell loss resulting from electrostatic cell attachment to tubes and the RNAse A to digest the double-stranded sections of RNA that might stain with PI. Measurements were done on a flow cytometer with an excitation of a 488-nm argon-ion laser line. The data were analyzed using the ModFitLT version 2.0 (PMac) DNA content histogram deconvolution software.

Table 1. Percentage of apoptosis in MDCK cells transfected with pGW1-HA-ZO-2

Transfection	Staurosporine	Viable cells (%)	Apoptotic early cells (%)	Apoptotic late cells (%)	Necrotic cells (%)
Mock		92.80 ± 0.64	0.20 ± 0.05	0.98 ± 0.09	6.03 ± 0.69
	0.5μM,4h	79.14 ± 2.58	1.31 ± 0.07	7.53 ± 0.45	12.03 ± 2.21
	1.0μM,24h	16.65 ± 1.90	0.57 ± 0.04	49.20 ± 5.50	33.50 ± 4.90
pGW1		90.85 ± 1.57	0.33 ± 0.12	1.37 ± 0.52	7.47 ± 0.96
pGW1-HA-ZO-2		92.75 ± 1.0	0.22 ± 0.07	1.18 ± 0.26	5.85 ± 0.72

Sparse MDCK cells were synchronized by serum starvation for 48 h. Then, they were incubated for 24 h in CDMEM and transfected with the empty vector or pGW1-HA-ZO-2. Twenty-four hours later, apoptosis was determined by annexin V fluorescence and flow cytometry. A group of nontransfected cells was treated with staurosporine for a positive apoptosis control. Media ± SE were obtained with the values from four independent experiments.

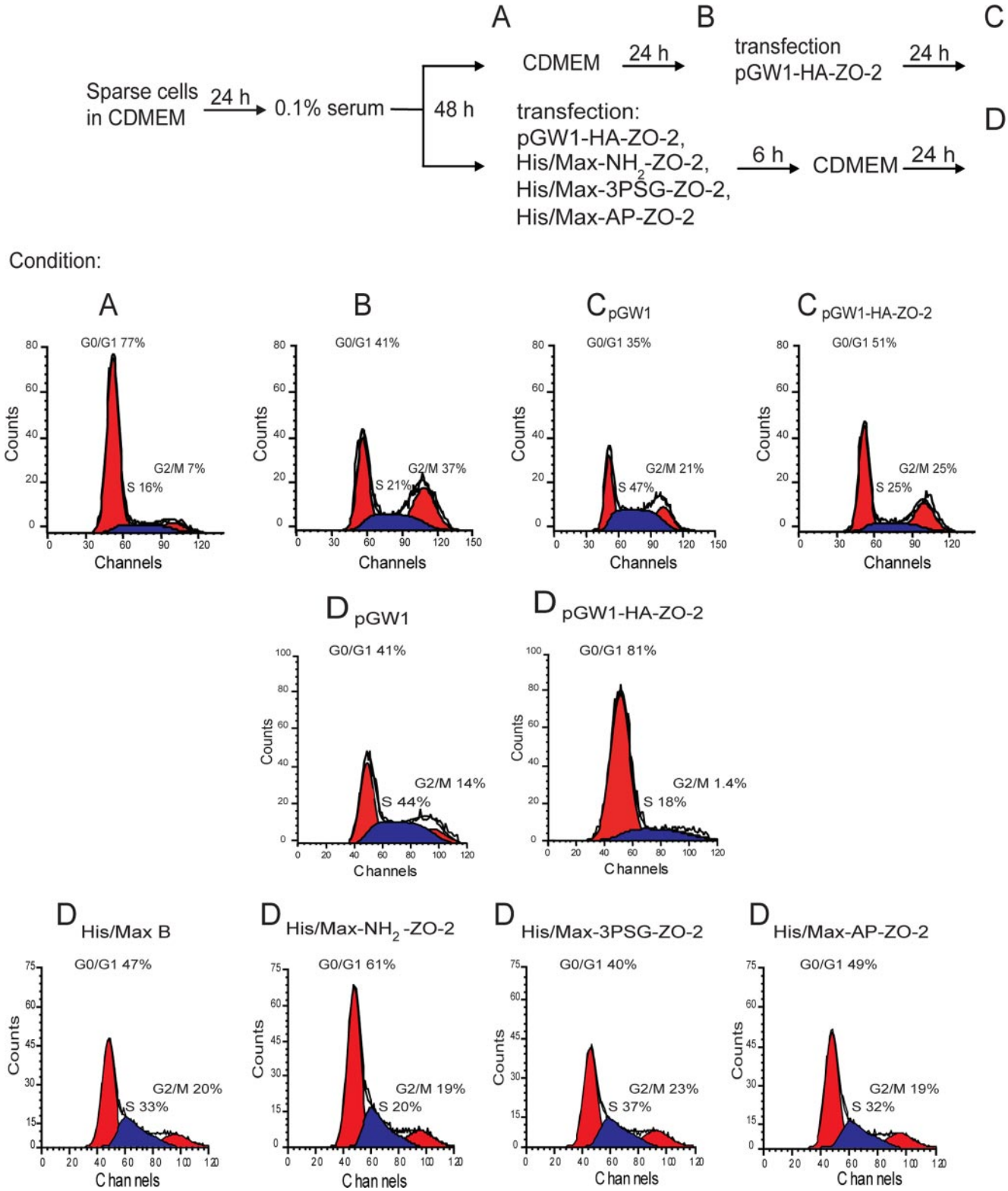

Figure 3. Flow cytometric analysis reveals a blockade at G0/G1 in cells transfected with ZO-2. Sparse cells incubated for 48 h with 0.1% serum (A), and further cultured for 24 h with CDMEM (B), were transfected with ZO-2 or the empty vector. After 24 h, the cells were stained with PI, and a flow cytometric analysis was performed (C) to obtain the percentages of cells in each particular stage of the cell cycle. Sparse cells incubated for 48 h with 0.1% serum (A) and then transfected with full-length ZO-2, the amino-, middle, and carboxy-terminal segments of ZO-2 or the empty vectors were incubated 6 h after the transfection with CDMEM. After 24 h, the cells were stained with PI, and a flow cytometric analysis was performed (D) to obtain the percentages of cells in each particular stage of the cell cycle. The upper portion of the figure illustrates the protocols used, whereas the lower section shows representative histograms obtained for each condition. The letters A, B, C, and D indicate the time point at which the distribution of cells in the particular stages of the cell cycle was evaluated.

Cell Proliferation Assay

The entry into the S phase was quantified by determining the incorporation of [^{3}H]thymidine. For this purpose, synchronized cells, transfected with pGW1-HA-ZO-2 or the empty vector, were incubated for 24 h with 0.45 μCi/ml [^{3}H]thymidine. The incorporation was stopped with two washes with cold PBS, precipitation with 5% (wt/vol) trichloroacetic acid, and cells were lysed with 0.4 M NaOH. After 1 h of gentle agitation at room temperature, 100 μl of each sample was taken for protein quantification, and another 100 μl was solubilized in 25 μl of 10% (vol/vol) acetic acid, 400 μl of 0.4 M NaOH, and 2 ml of scintillation liquid. Samples were counted in a beta-scintillation counter (LS 6000 TA; Beckman Coulter, Fullerton, CA).

Cell Viability and Apoptosis Determination

The proportion of viable cells in the culture was determined using the vital stain trypan blue (Sigma-Aldrich), according to the manufacturer's instructions.

Translocation of phosphatidylserine (PS) to the external surface of the membrane was determined using the annexin V-FLUOS staining kit (Roche Diagnostics), according to the manufacturer's instructions. Wild-type MDCK cells, treated for 4 h with 0.5 μM staurosporine or for 24 h with 1.0 μM staurosporine, were used as a positive control for apoptosis induction. The percentage of early apoptotic and lysed apoptotic cells was determined on a BD Biosciences fluorescence-activated cell sorting (FACS) Vantage SE BD system (BD Biosciences, San Jose, CA).

Immunofluorescence

Monolayers grown on glass coverslips were fixed with 2% (wt/vol) *p*-formaldehyde in PBS, pH 7.4, and permeabilized for 5 min with 0.1% (vol/vol) Triton X-100 in PBS. Cells were washed five times with PBS and then blocked for 30 min with 1% (wt/vol) bovine serum albumin (Ig-free) (1331-a; Research Organics, Cleveland, OH) containing 0.03% (wt/vol) saponin. The monolayers were incubated overnight at 4°C with rabbit polyclonal anti-ZO-2 antibodies (71-1400; Zymed Laboratories) (diluted 1:100) or anti-CD1 (Sc-717; Santa Cruz Biotechnology) (diluted 1:50).

After five times washing with PBS, the coverslips were incubated for 1 h at room temperature with fluorescein isothiocyanate -conjugated goat-anti-rabbit antibody (65-6111; Zymed Laboratories) (diluted 1:100). After a three times wash, the monolayers on glass coverslips were mounted with the antifade reagent VECTASHIELD (H-1000; Vector Laboratories, Burlingame, CA). The fluorescence of the monolayers was examined using a SP2 confocal microscope (Leica, Wetzlar, Germany) with argon and helium-neon lasers and using the Leica confocal software.

Quantitative Reverse Transcription-Polymerase Chain Reaction (qRT-PCR)

Total RNA was extracted from cells using the TRIzol reagent (Invitrogen). qRT-PCR was performed by a two-step method. cDNA was generated from 1 μg of total RNA by Improm-II reverse transcription system (Promega) with oligo(dT)$_{15}$ as a primer according to the manufacturer's instruction. PCR was performed with the QuantiTect SYBR Green PCR kit (204143; QIAGEN, Hilden, Germany) in a volume of 25 μl. Triplicate samples were subjected to qPCR by using the 7300 Real-Time PCR System (Applied Biosystems, Foster City, CA), with the maximum cycle number of 40. Actin was used as an internal control. The relative abundance of cyclin D1 gene expression was calculated. Two independent batches of RNA samples were used for qRT-PCR analysis, and data were present as mean ± SE and analyzed by Student's *t* test.

qPCR profile consisted of an initial denaturation step at 95°C for 10 min followed by 40 cycles of denaturation at 95°C for 30 s, annealing at 60°C for 1 min, and extension 72°C for 30 s. A dissociation step was added. No amplification was detected for controls without template.

The -fold differences in expression levels were calculated according to the $2^{-\Delta\Delta CT}$ method. To study the effects of ZO-2 on endogenous expression of *axin-2*, *MMP14*, and *p53*, SW480 and MCF-7 cells were transiently transfected with 2 μg of HA-pGW 1 or HA-pGW 1 ZO-2 plasmid by using FuGENE HD (Roche Diagnostics). After 12 h total RNA was isolated with the NucleoSpin RNA/protein kit (Macherey & Nagel, Düren, Germany), and reverse transcription was performed with the High-Capacity cDNA Reverse Transcription kit (Applied Biosystems, Darmstadt, Germany). Real-time PCR was performed by using *Taq*Man Gene Expression assays HS00610344_m1 (*axin2*), HS01037009_g1 (*MMP14*), and HS00153349_ml (*p53*), with unlabeled primers and FAMdye-labeled MGB probes. Human β-actin (unlabeled primer, VIC/TAMRA dye-labeled probe; Applied Biosystems) served as endogenous control and was not affected under experimental conditions. Each PCR was set up in duplicates, and threshold cycle (Ct) values of the target genes were normalized to the endogenous control. Differential expression was calculated according to the $2^{-\Delta\Delta CT}$ method (Livak and Schmittgen, 2001).

Biosynthetic Labeling

Subconfluent MDCK cells incubated for 48 h in serum-deprived media (0.1% (vol/vol) serum) were transfected with full-length ZO-2; His-NH$_2$-ZO-2 construct; full-length ZO-1; the corresponding empty vectors pGW1, pHis/MaxB, and pCB6; or ZO-2 siRNA and the negative control NC. Six hours after transfection, the cells were transferred to CDMEM, and after 24 h, cells were incubated in methionine- and cysteine-free Dulbecco's modified Eagle's medium (catalog no. 010909; In Vitro, Mexico D.F.) containing 4 mM glutamine, 5 μg/ml insulin, and 5% (vol/vol) dialyzed fetal bovine serum for 30 min and labeled with 100 μCi of Easy Tag Express protein labeling mix [^{35}S]Met/Cys (PerkinElmer Life and Analytical Sciences, Boston, MA) for different times (45–120 min). The radioactive medium was removed, and the cells were washed three times with ice-cold PBS and treated with a lysis buffer [10 mM Tris-HCl, pH 7.6, 150 mM NaCl, 1% (wt/vol) sodium deoxycholate, 0.1% (wt/vol) SDS, 1% (vol/vol) NP-40, and 1 mM PMSF] containing the protease inhibitor cocktail Complete. The amount of protein was quantified and 600 μg of cell lysate derived from ZO-2, ZO-1, or empty vector-transfected cells were

Table 2. Percentage of cells found at the different stages of the cell cycle in synchronized cultures transfected with full length ZO-2 or with ZO-2 segments

			Synchronized cells							
			C (%)		D (%)					
Cell cycle stage	A (%)	B (%)	pGW1	pGW1-HA-ZO-2	pGW1	pGW1-HA-ZO-2	His/Max	His-NH$_2$-ZO-2	His-3PSG-ZO-2	His-AP-ZO-2
G0/G1	73 ± 0.19	48 ± 3.0	34 ± 0.8	48 ± 1.5	45 ± 1.3	70 ± 2.8 ***	48 ± 3.0	61 ± 0.6 **	44 ± 2.2	50 ± 1.9
S	16 ± 0.37	23 ± 1.0	46 ± 0.7	28 ± 1.7	24 ± 0.7	13 ± 1.5 *	29 ± 2.9	24 ± 2.5 *	34 ± 4.0	31 ± 4.1
G2/M	11 ± 0.36	29 ± 3.0	20 ± 0.6	24 ± 1.2	31 ± 1.1	17 ± 3.5 ***	23 ± 3.7	15 ± 2.7	22 ± 3.4	19 ± 2.4

The letters A, B, C, and D indicate the moment at which the distribution of cells in the particular stages of the cell cycle was evaluated, according to the protocol illustrated in the diagram of Figure 3. Cells evaluated at the C and D condition were transfected with pGW1-HA-ZO-2 or the empty vector. Media ± SE were obtained with the values from four independent experiments (*p ≤ 0.05; **p ≤ 0.01, and ***p ≤ 0.001; ANOVA Tukey's multiple comparison test).

used to CD1 immunoprecipitation. Immunoprecipitates were resolved on 12% SDS-polyacrylamide gel electrophoresis (PAGE) gels and ^{35}S-labeled proteins were detected on dried gels and quantified using the Personal Molecular Imager FX phosphorimaging system (Bio-Rad, Hercules, CA).

Analysis of CD1 Stability

Sparse cultures of MDCK cells synchronized by serum starvation for 48 h were transfected with full-length ZO-2; His-NH_2-ZO-2 construct; full-length ZO-1; the corresponding empty vectors pGW1, His/MaxB, and pCB6; or ZO-2 siRNA and the negative control NC. After 24 h, the cells were incubated in methionine- and cysteine-free DMEM containing 4 mM glutamine, 5 μg/ml insulin, and 5% (vol/vol) dialyzed fetal bovine serum for 30 min and then labeled with 100 μCi of Easy Tag Express protein labeling mix [^{35}S]Met/Cys. To determine the rate of turnover of CD1, the radioactive medium was removed 1 h after addition, and the cells were then rapidly washed with a large volume of CDMEM and incubated for different chase periods (45, 60, 90, and 120 min) at 37°C with CDMEM containing 50 μg/ml cyloheximide an inhibitor of protein synthesis. The cells were next harvested for CD1 immunoprecipitation and the immunoprecipitates were resolved on 12% SDS-PAGE gels. ^{35}S-labeled proteins were detected on dried gels and quantified with the Personal Molecular Imager FX phosphorimaging system (Bio-Rad).

Inhibition of Protein Degradation

Sparse cells synchronized by serum starvation for 48 h and subsequently cultured in CDMEM for 24 h were transfected with pGW1-HA-ZO-2 or the empty vector. Eight hours later, the cells were treated for 16 h with 50 mM LiCl, an inhibitor of GSK-3β. Alternatively, 19 h after transfection, the cultures were incubated for 5 h with 50 μM MG132, a proteosomal inhibitor, or 100 μM cloroquine, a lysosomal inhibitor. Then, the cells were lysed and processed for SDS-PAGE and blotted with specific antibodies against ZO-2, CD1, and actin.

RESULTS

Overexpression of ZO-2 Down-Regulates Cyclin D1 Protein and Inhibits Cell Proliferation

To investigate the role of ZO-2 on cell proliferation, epithelial cells were transfected with increasing amounts of ZO-2 expression vector, and changes in CD1 protein levels were analyzed by Western blotting (Figure 1). Concomitant with the increase of ZO-2 protein levels, the amount of CD1 protein decreases.

Next, we evaluated the impact of ZO-2 overexpression on cell proliferation. As shown in Figure 2A, in synchronized cultures of sparse cells, ZO-2 transfection inhibits [^{3}H]thymidine incorporation, whereas no effect was detectable in confluent cultures, which as expected exhibited a low [^{3}H]thymidine incorporation rate. The diminished incorporation of [^{3}H]thymidine is not due to an increased rate of cell death, because ZO-2 transfection does not change the cell viability, as determined by trypan blue exclusion (Figure 2B). Moreover, ZO-2 transfection does not augment the percentage of necrotic, early, or late apoptotic cells in the culture (Table 1), as analyzed with an annexin assay by flow cytometry. In these experiments, staurosporine, a potent protein kinase C inhibitor (Tamaoki *et al*., 1986), frequently used as an apoptosis inductor (Nicotera *et al*., 1999; Zamorano *et al*., 2004), was included as a positive control for apoptosis induction.

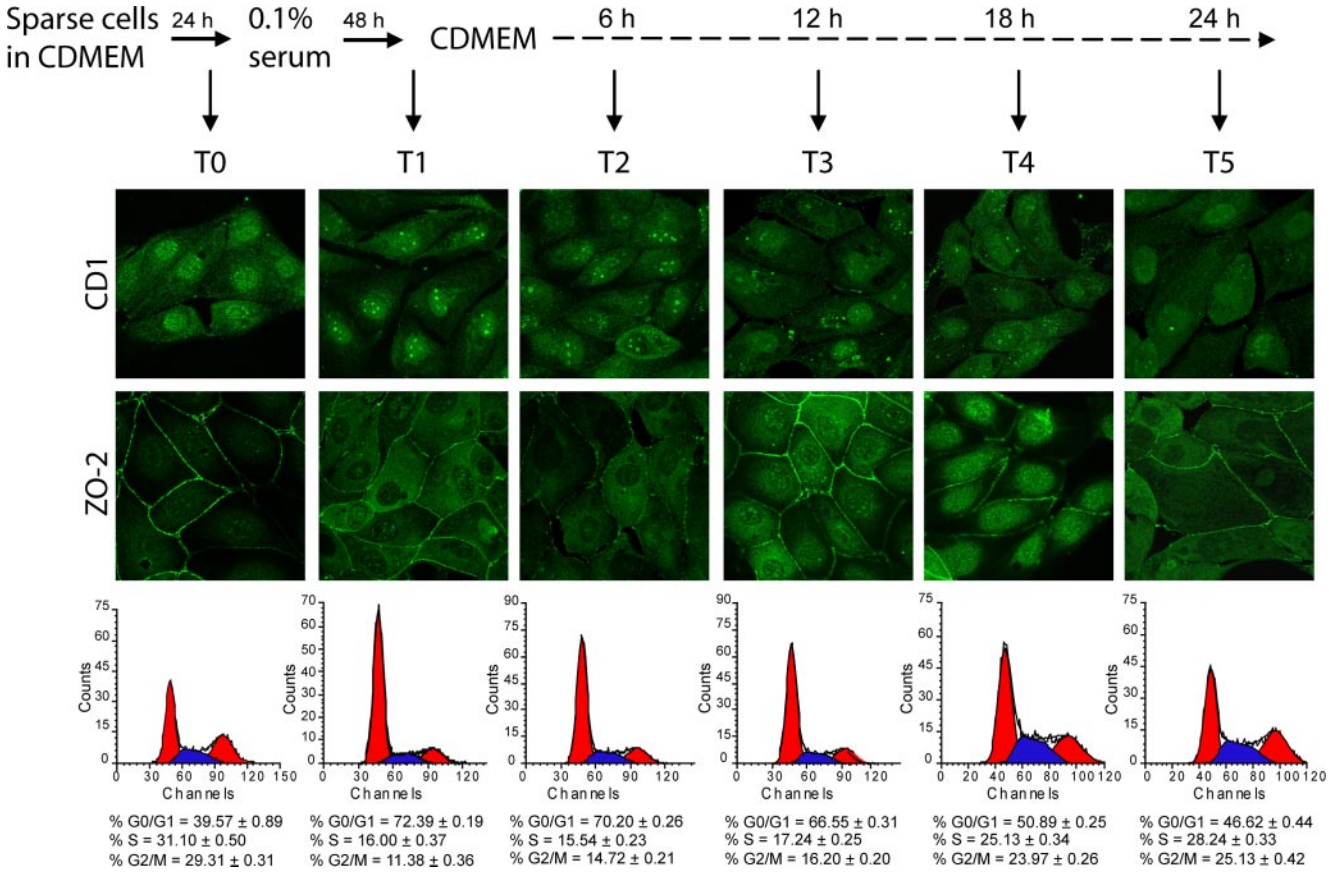

Figure 4. Release of synchronized cell cultures into the cell cycle changes the subcellular distribution of CD1 and ZO-2. Immunofluorescence microscopic detection of ZO-2 and CD1, and flow cytometric analysis were done in parallel at different times, indicated in the upper diagram, in serum-deprived cells and in those subsequently transferred to the normal growth media CDMEM. At least two independent experiments were performed for each time.

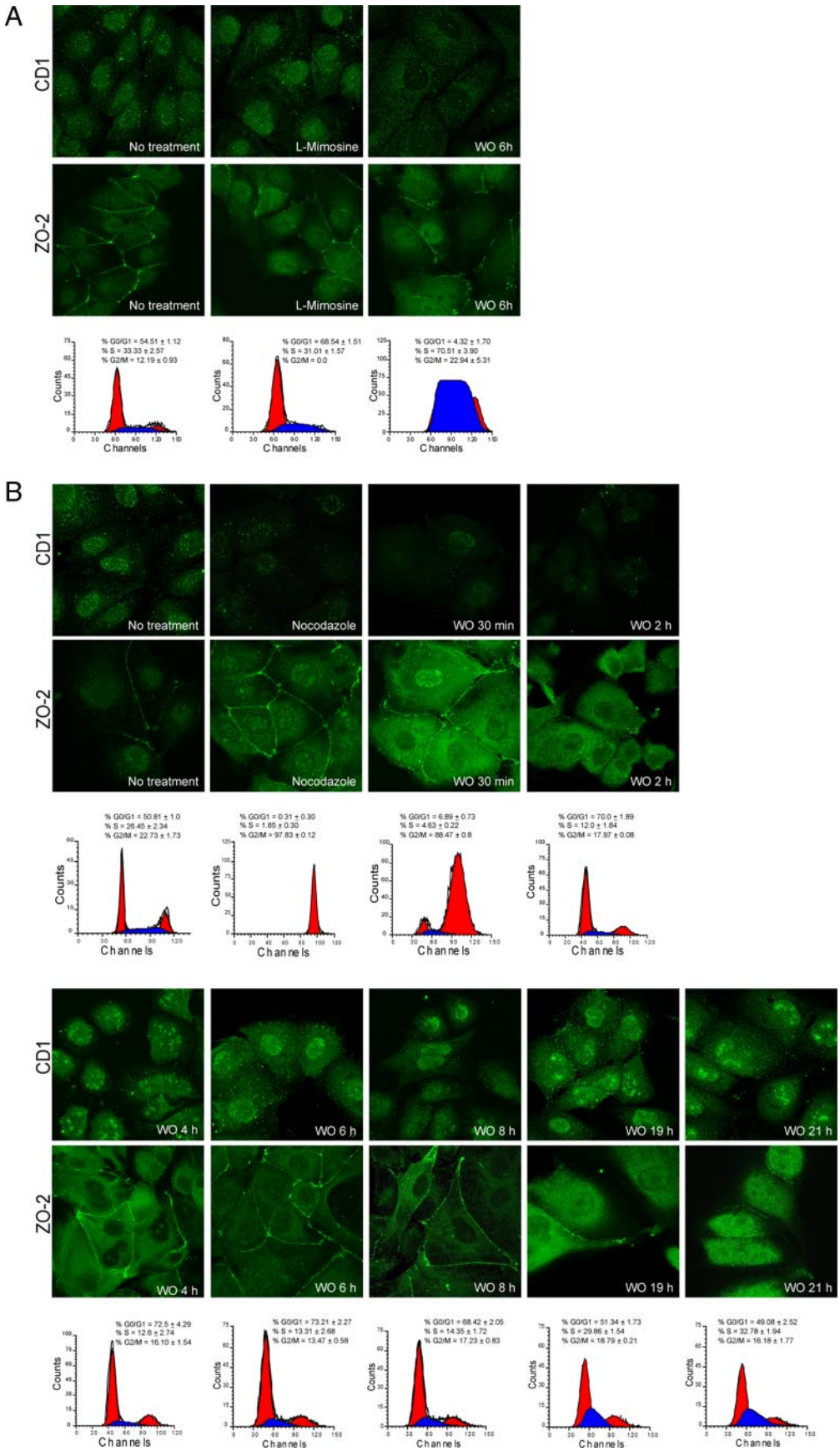
A
CD1
ZO-2
No treatment
L-Mimosine
WO 6h
% G0/G1 = 54.51 ± 1.12
% S = 33.33 ± 2.57
% G2/M = 12.19 ± 0.93
% G0/G1 = 68.54 ± 1.51
% S = 31.01 ± 1.57
% G2/M = 0.0
% G0/G1 = 4.32 ± 1.70
% S = 70.51 ± 3.90
% G2/M = 22.94 ± 5.31
Counts
Channels
B
CD1
ZO-2
No treatment
Nocodazole
WO 30 min
WO 2 h
% G0/G1 = 50.61 ± 1.0
% S = 26.45 ± 2.34
% G2/M = 22.73 ± 1.73
% G0/G1 = 0.31 ± 0.30
% S = 1.85 ± 0.30
% G2/M = 97.83 ± 0.12
% G0/G1 = 6.89 ± 0.73
% S = 4.63 ± 0.22
% G2/M = 88.47 ± 0.8
% G0/G1 = 70.0 ± 1.89
% S = 12.0 ± 1.84
% G2/M = 17.97 ± 0.08
WO 4 h
WO 6 h
WO 8 h
WO 19 h
WO 21 h
% G0/G1 = 72.5 ± 4.29
% S = 12.6 ± 2.74
% G2/M = 16.10 ± 1.54
% G0/G1 = 73.21 ± 2.27
% S = 13.31 ± 2.68
% G2/M = 13.47 ± 0.58
% G0/G1 = 68.42 ± 2.05
% S = 14.35 ± 1.72
% G2/M = 17.23 ± 0.83
% G0/G1 = 51.34 ± 1.73
% S = 29.86 ± 1.54
% G2/M = 18.79 ± 0.21
% G0/G1 = 49.08 ± 2.52
% S = 32.78 ± 1.94
% G2/M = 16.18 ± 1.77

Figure 5.

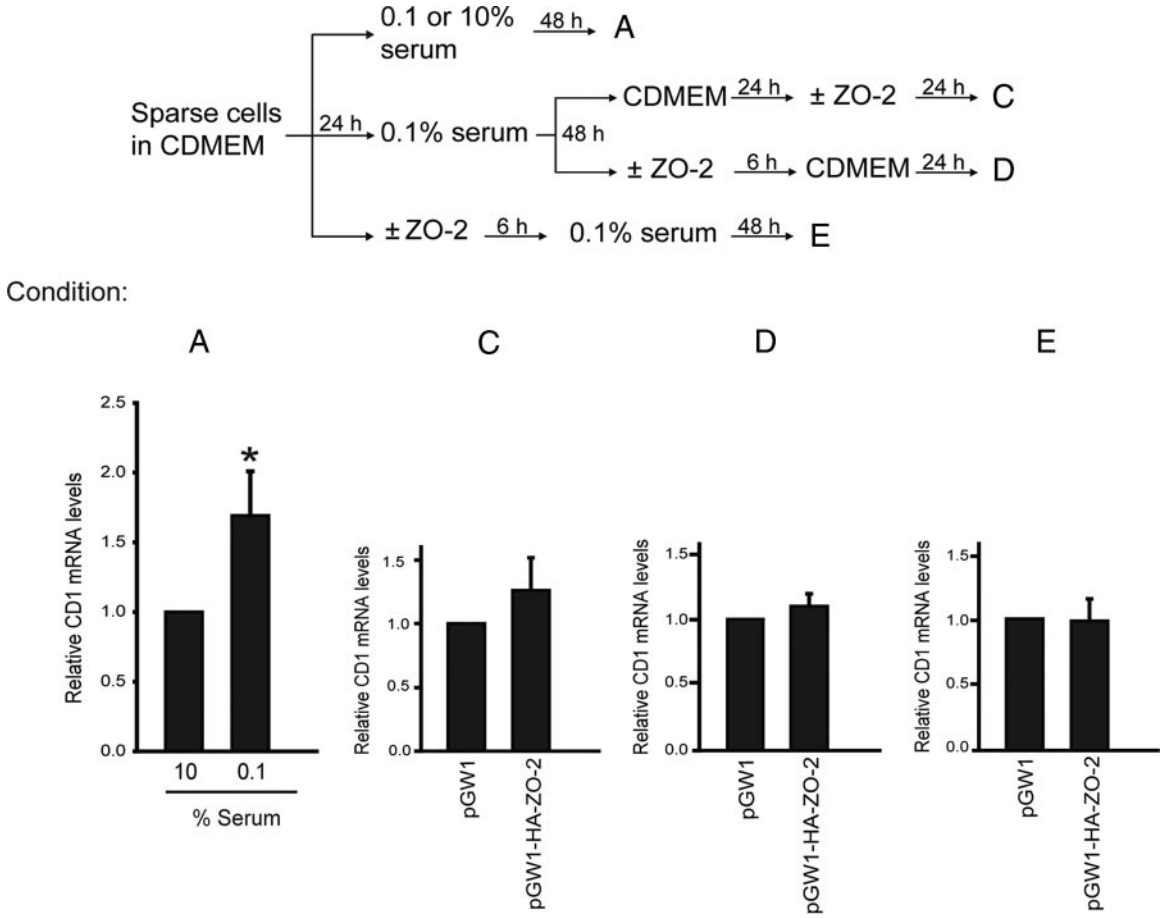

Figure 6. ZO-2 overexpression exerts no effect on the level of CD1 mRNA in synchronized cultures. Quantitative RT-PCR experiments were performed at the times indicated with the letters A, C, D, and E in epithelial cells that were treated as schematically depicted in the upper portion of the figure. The results obtained with two independent experiments are presented in the lower histograms.

ZO-2 Overexpression Blocks Cell Cycle Progression

Because ZO-2 overexpression inhibits cell proliferation, we next explored in which stage of the cell cycle the cells were arrested. To test the impact of ZO-2 on cell cycle progression, we used two protocols using cell cultures synchronized by serum deprivation. The letters A, B, C, and D in Figure 3 indicate the time at which the cell cycle distribution of cells was evaluated by flow cytometric analysis. Figure 3 shows a representative example of the DNA content frequency histograms, whereas the values of three to seven independent experiments are summarized in Table 2.

After 48 h of incubation in media with 0.1% of serum 77% of cells were arrested at G_0/G_1 (condition A). The subsequent transfer for 24 h to CDMEM triggers the entry of the synchronized culture into the cell cycle, reducing the percentage of cells at G0/G1 to 41% (condition B). If at this point the cells are transfected with ZO-2, it was observed that 24 h later (condition C), the percentage of cells at G0/G1 further increases to 51%, whereas in control cells treated with empty vector, only 35% of cells were at G0/G1. In the second protocol, we transfected the cells with ZO-2 after 48 h of incubation in medium containing 0.1% serum (condition A) and before adding CDMEM for 24 h to the serum-deprived cultured cells. Under these conditions, the percentage of cells transfected with ZO-2 displayed a significantly higher amount of cells at G0/G1 than those transfected with the empty vector (81 vs. 41%; condition D). Together, these results indicate that the overexpression of ZO-2 inhibits the progression of cells through the cell cycle at the G1/S boundary.

Next, we analyzed which part of ZO-2 was responsible for inhibiting cell cycle progression. For this purpose, the monolayers following condition D were transfected with constructs encoding the amino-terminal (His-NH_2-ZO-2), middle (His-3PSG-ZO-2), and carboxy-terminal (His-AP-ZO-2) segments of ZO-2, or with the corresponding empty vector (His/MaxB). Transfection with the middle and carboxy-terminal segments of ZO-2 exerted no significant effect. In contrast, transfection of the ZO-2 amino-terminal fragment increased the percentage of cells at G0/G1 in comparison with cultures transfected with the empty vector (61 vs. 47%).

Figure 5 (cont). The nuclear distribution of ZO-2 and CD1 is sensitive to the cell cycle status. Immunofluorescence detection of ZO-2 and CD1 in (A) MDCK cells either not treated or treated with 1 mM L-mimosine for 24 h. Subsequently, cells were either fixed or the drug was washed out and cells were incubated for further 6 h in normal growth media (CDMEM) and then fixed. (B) Cultures treated or untreated with 0.3 μM nocodazole for 16 h were treated as described above and then fixed after the drug had been washed out for different times. At the bottom part of each panel of this figure, a flow cytometric analysis reveals the percentages of cells found in each particular stage of the cell cycle. At least two independent experiments were done for each time point.

The value obtained is lower, albeit of no statistical difference to that obtained after transfection with full length ZO-2 (Table 2).

The Subcellular Localization of ZO-2 and Cyclin D1 Varies within the Cell Cycle

Next, we studied the subcellular distribution of CD1 in response to ZO-2 overexpression. Immunofluorescence microscopy (IF) did not reveal any changes in the nuclear localization of CD1 (data not shown). Therefore, in a next set of experiments, we decided to analyze the distribution of endogenous ZO-2 and cyclin D1 during the cell cycle. As illustrated in Figure 4, in cultures synchronized by serum starvation, transfer to CDMEM induces an increase in CD1 nuclear staining, as the cells moves through the cell cycle. This effect is even more evident for ZO-2 as in serum-deprived cells ZO-2 nuclear staining is low, whereas after 18 h a strong nuclear staining was detectable. Membrane staining of ZO-2 does no change through the cell cycle. To explore the location of CD1 and ZO-2 in a condition where a higher percentage of cells is in a particular phase of the cell cycle pharmacological agents were used. For this purpose, sparse nonsynchronized cells were treated with L-mimosine, a plant amino acid derivative that blocks cell cycle progression in the late G1 phase (Krude, 1999). After a 24-h treatment with 1 mM L-mimosine, one group of cells was fixed and processed for immunofluorescence (IF) detection of ZO-2 and CD1, whereas in other monolayers the drug containing media was washed out, and incubation was continued in normal growth media for 6 h after which the IF procedure was performed. As shown in Figure 5A, in cultures treated with L-mimosine, 69% of the cells are at G1 phase. The IF observation shows a slight increase in CD1 nuclear staining and no obvious difference in the distribution and extent of nuclear ZO-2 in comparison with untreated cells. In contrast, 6 h after the washout of L-mimosine from the culture media, 71% of the cells are in the S phase and CD1 nuclear staining is no longer detectable, whereas ZO-2 is still present in the nucleus. Next, sparse unsynchronized cultures were treated for 16 h with 0.3 μM nocodazole. This agent arrests the cell cycle at the beginning of mitosis because it blocks spindle microtubule assembly but permits other mitotic events to proceed such as chromosome condensation and cell rounding (Hamilton and Snyder, 1982). Figure 5B illustrates that in cultures treated with nocodazole 98% of cells are at G2/M and ZO-2 exhibits a conspicuous nuclear staining, whereas the nuclear CD1 signal is low. After a 30-min washout, ZO-2 disappears from the nucleus. At this time, the percentage of cells that has reached the G0/G1 phase is still very low (7%), indicating that ZO-2 exits the nucleus at mitosis. Four hours after the nocodazole washout, CD1 is conspicuously present at the nucleus. Because FACS analysis revealed that at this time the percentage of cells at G0/G1 has increased to 73%, these results suggest that CD1 enters the nucleus at the early stages of G1. Nineteen hours after washout, when the percentage of cells at G0/G1 has diminished to 51% and that at S has increased to 30%, ZO-2 is present at the nucleus. This observation together with that obtained with mimosine treatment strongly suggests that ZO-2 enters the nucleus at the later stages of G1.

ZO-2 Overexpression Exerts No Effect on the Level of CD1 mRNA in Synchronized Cultures

Because the presence of CD1 is necessary for cell cycle progression through G1 to S phase we next explored, by quantitative RT-PCR, if ZO-2 transfection affected the amount of CD1 mRNA. The letters A, C, D, and E indicate the time at which the mRNA was harvested and qRT-PCR was performed for each experimental condition as schematically depicted in the diagram of Figure 6. Results obtained in two independent experiments are summarized in the lower histograms.

Transfection of ZO-2 to a synchronized cell culture has no impact on the amount of CD1 mRNA (condition C) even if ZO-2 is transfected before the cells are switched to serum-containing media (condition D) (Figure 6). Interestingly, the amount of CD1 mRNA is higher in cells incubated for 48 h in 0.1% serum than in those cultured with CDMEM (condition A), and transfection of ZO-2 to cells that are subsequently incubated in serum-deprived media exerts no change in the amount of CD1 mRNA (condition E). Together, these results indicate that in cells

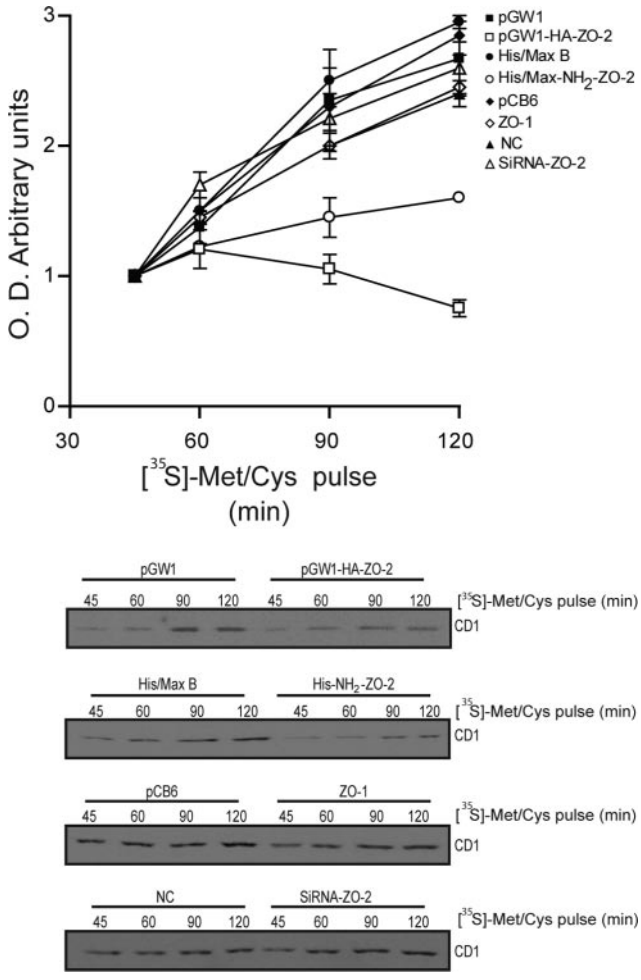

Figure 7. ZO-2 transfection specifically inhibits CD1 synthesis. MDCK cells synchronized by serum deprivation for 48 h were transfected with full-length ZO-2; His-NH_2-ZO-2 construct; full-length ZO-1; the corresponding empty vectors pGW1, His/MaxB, and pCB6; or ZO-2 siRNA and the negative control NC, and then transferred to CDMEM for 24 h. Subsequently, the cells were labeled with [^{35}S]Met/Cys for the indicated times. ^{35}S labeling of immunoprecipitated CD1 derived from an equal amount of protein from each of the culture lysates was quantified by SDS-PAGE and phosphorimaging. A gel from one experiment and the quantitative results obtained from two to four independent experiments are shown.

that have been synchronized by serum deprivation ZO-2 transfection exerts no effect on the level of CD1 mRNA in comparison with cultures transfected with the empty vector.

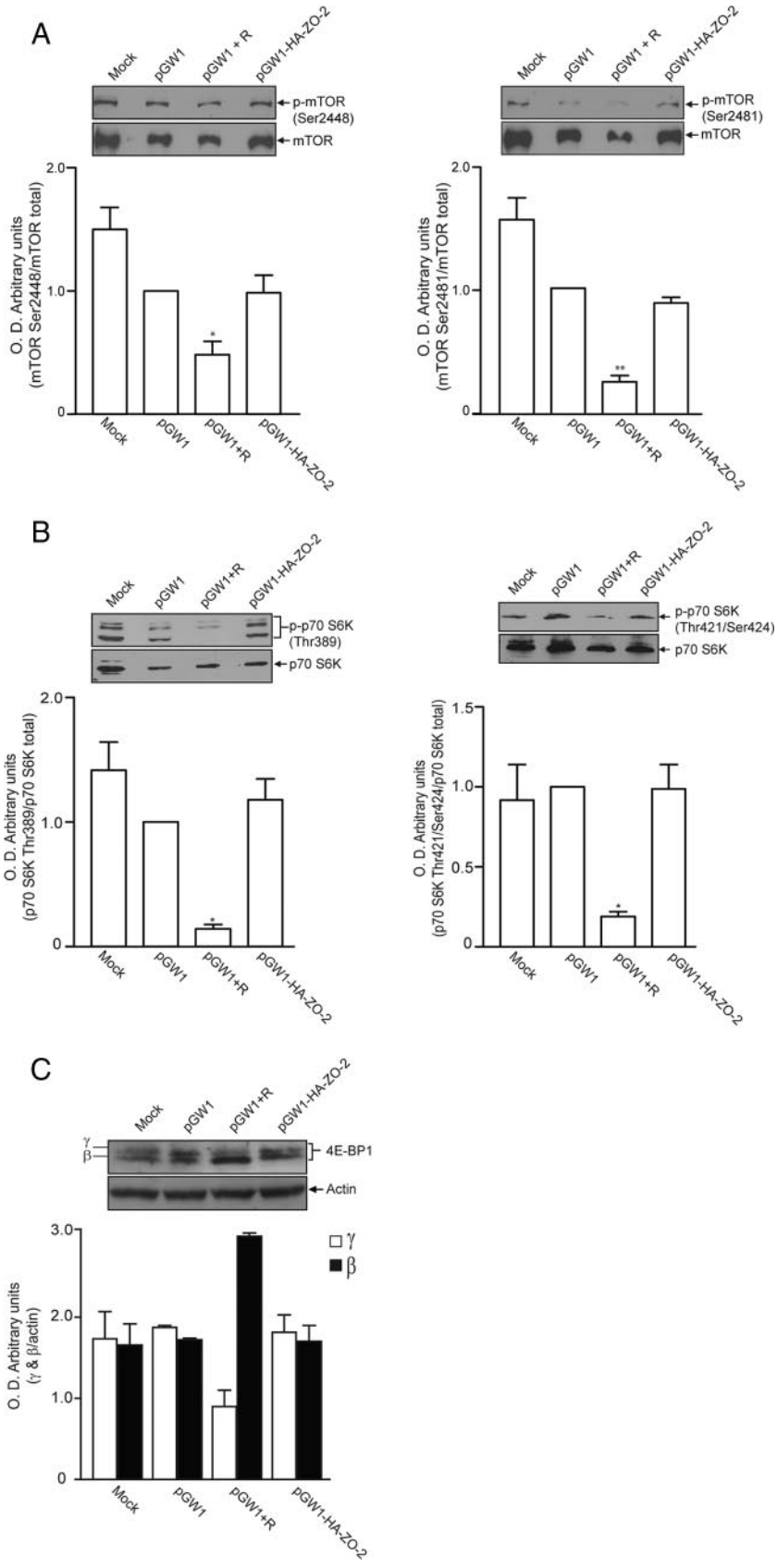

Figure 8. ZO-2 overexpression has no effect on the phosphorylation of mTOR and its targets p70 S6K and 4E-BP1. MDCK cells synchronized for 48 h by serum deprivation were incubated for 24 h in CDMEM and subsequently transfected with ZO-2 or the empty vector. After 24 h, the cells were lysed and processed for SDS-PAGE. Some cultures were treated with rapamycin (R) for 30 min before cell lysis. Western blots were done with antibodies against: mTOR and phosphorylated Ser2448 or Ser2481 of mTOR (A), p70 S6K and phosphorylated Thr389 and Thr421/Ser424 of p70 S6K (B), and 4E-BP1 and actin (C).

ZO-2 Overexpression Inhibits CD1 Synthesis

Because ZO-2 overexpression decreases the amount of CD1 protein present in MDCK cells, but exerts no effect on the level of CD1 mRNA, we proceeded to analyze the impact of ZO-2 on CD1 synthesis. For this purpose, [^{35}S]Met/Cys labeling for different times was performed in cells transfected with ZO-2 or the empty vector pGW1 (condition D in Figure 3). As presented in Figure 7, a significantly lower radioactive labeling of immunoprecipitated CD1 in cells transfected with ZO-2 relative to those transfected with the empty vector at 90 and 120 min was detectable. Next, we analyzed whether these effects are specific for ZO-2. For such a purpose, the cells were transfected with ZO-1, another MAGUK TJ protein, and with a ZO-2 siRNA shown previously by us to specifically inhibit ZO-2 expression (Hernandez *et al*., 2007). As controls, cells were transfected with the empty vector pCB6 and NC, which corresponds to a siRNA without any homology to any sequence in the vertebrate transcriptome. Figure 7 illustrates that ZO-2–induced effects upon CD1 de novo synthesis are specific because the overexpression of ZO-1 did not exert a comparable effect. Similarly depletion of ZO-2 by siRNA did not affect CD1 synthesis in accordance with previous results showing that ZO-2 silencing has no impact on cell proliferation (Hernandez *et al*., 2007).

Because transfection with the amino-terminal fragment of ZO-2 increases the percentage of cells at G0/G1, we next explored its impact on de novo CD1 synthesis. Cells transfected with His-NH_2-ZO-2 revealed a significantly lower radioactive labeling of immunoprecipitated CD1 in monolayers than cells in cultures treated with the empty vector (His/MaxB) (Figure 7). Together, these results suggest that ZO-2 overexpression specifically inhibits the translation of CD1

To determine whether ZO-2 specifically blocks CD1 synthesis or instead is capable of inhibiting the overall protein synthesis, we proceeded to analyze the effect of ZO-2 transfection on the phosphorylation of mTOR and its targets. mTOR (Sabers *et al*., 1995), also known as FRAP or RAFT (Brown *et al*., 1994; Sabatini *et al*., 1994), is a Ser/Thr protein kinase that plays a major role in regulating cell growth through the control of protein synthesis (Dennis *et al*., 2001; Fang *et al*., 2001). When sufficient nutrients are available mTOR is phosphorylated at Ser2448 via the phosphatidylinositol 3-kinase/Akt signaling pathway (Nave *et al*., 1999) and is autophosphorylated at Ser2481 (Peterson *et al*., 2000). mTOR phosphorylates two translational regulatory proteins: the 40S ribosomal protein p70 S6 kinase (p70 S6 K) and the eukaryotic initiation factor 4E-binding protein (4E-BP1) (Gingras *et al*., 1999). 4E-BP1 binds eukaryotic initiation factor (eIF) 4E thereby inhibiting cap dependent translation. Phosphorylation of 4E-BP1 by mTOR disrupts this binding and in consequence activates cap-dependent translation.

As shown in Figure 8A, the phosphorylation of mTOR at Ser2448 and Ser2481 is unaffected by ZO-2 transfection, whereas the system is sensitive to rapamycin, an antifungal agent that specifically inhibits mTOR (Sabers *et al*., 1995). In a similar manner, mTOR phosphorylation targets p70 S6K and 4E-BP1, exhibit no changes upon ZO-2 transfection but are responsive to rapamycin treatment. In Figure 8B, we used antibodies against the phosphorylated residues Thr389 and Thr421/Ser424 of p70 S6K that are phosphorylated upon mTOR activation (Pullen and Thomas, 1997; Polakiewicz *et al*., 1998). For the experiment depicted in Figure 8C, an antibody was used that detects bands β and γ, of 4E-BP1, which are phosphorylated to a different degree. Both mock-transfected cells and those transfected with ZO-2 or the empty vector exhibited the same pattern of 4E-BP1 bands, whereas as expected the cells treated with rapamycin show a lower amount of the highly phosphorylated γ band and an increased amount of the less phosphorylated β band. Together, these results suggest that ZO-2 overexpression does not affect the overall protein synthesis but specifically inhibits the translation of CD1.

Finally, we tested whether the inhibition of CD1 synthesis is associated with an increased phosphorylation of the translation elongation initiation factor eIF2α, but we obtained no significant change upon ZO-2 overexpression (data not shown).

ZO-2 Increases CD1 Protein Decay

Next, we decided to explore whether ZO-2 affects the stability of CD1. For this aim [^{35}S]Met/Cys pulse-chase analyses of CD1 protein degradation were performed. A steeper rate of decay of CD1 was detectable in cells transfected with ZO-2 (Figure 9). This effect seems to be specific for ZO-2 because transfection with ZO-1 elicits no change in CD1 decay. ZO-2 silencing also had no impact on CD1 turnover, whereas transfection with the ZO-2 amino-terminal segment accelerated CD1 decay similar to full-length ZO-2.

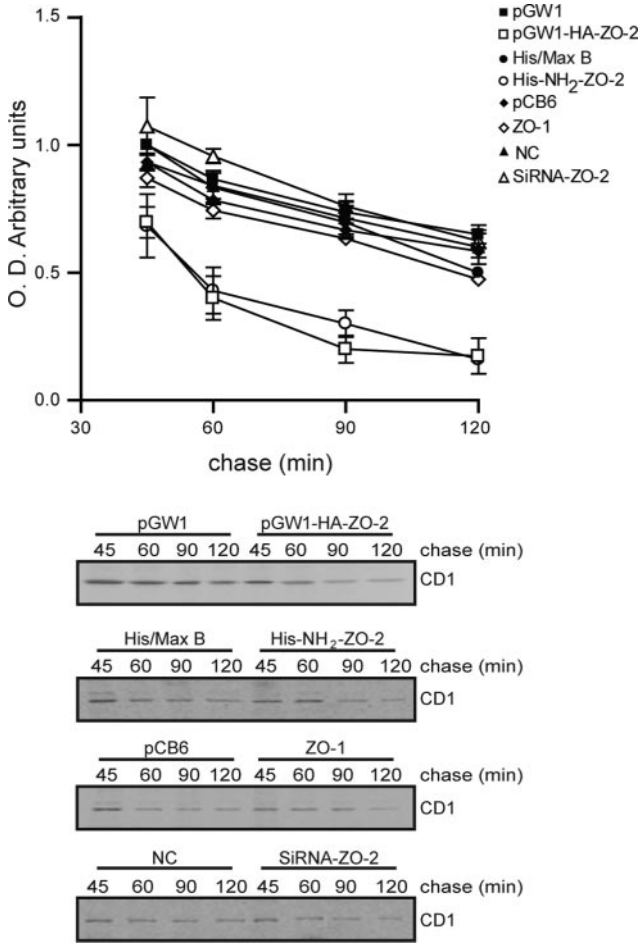

Figure 9. ZO-2 overexpression accelerates CD1 decay. MDCK cells synchronized by serum deprivation for 48 h were transfected with full-length ZO-2; His-NH_2-ZO-2 construct; full-length ZO-1; the corresponding empty vectors pGW1, His/MaxB; and pCB6; or ZO-2 siRNA and the negative control NC, and after 6 h they were transferred to CDMEM. After 24 h, the cells received a pulse of [^{35}S]Met/Cys. One hour later, the medium was removed, and the chase proceeded for the indicated times in the presence of cycloheximide.

ZO-2 Overexpression Decreases the Ser9 Inhibitory Phosphorylation of GSK-3β and Represses β-Catenin Target Genes Expression

Degradation of CD1 has been shown to be triggered by its phosphorylation by the Ser/Thr kinase GSK-3β. During S phase, a fraction of GSK-3β localizes to the nucleus, phosphorylates CD1 at Thr286 provoking its nuclear export, ubiquitination, and degradation by the 26S proteosome (Diehl *et al*., 1998; Gladden and Diehl, 2005). GSK-3β activity is inhibited by phosphorylation at Ser9 via several signal transduction pathways, including Akt, the mitogen-activated protein kinase cascade and mTOR (Cross *et al*., 1995; Frame and Cohen, 2001). To further analyze the effect of ZO-2 on CD1 degradation, we explored whether ZO-2 transfection affects the phosphorylation of GSK-3β at Ser9. Indeed, ZO-2 overexpression decreases GSK-3β Ser9 phosphorylation (Figure 10A).

GSK-3β is a central player in intracellular Wnt signal transduction (Frame and Cohen, 2001). In the absence of a Wnt signal, GSK-3β present in complex with the adenomatosis polyposis coli protein APC and the scaffold protein Axin phosphorylates cytosolic β-catenin, which is then ubiquitinated and degraded in proteasomes. In the presence of Wnt, β-catenin is not phosphorylated by GSK-3β; hence, β-catenin is translocated to the nucleus where it associates with the T cell factor transcription factor to control the expression of particular target genes that include among others the homeobox gene siamois that regulates the early dorsal axis specification in embryos (Brannon *et al*., 1997).

To further explore the impact of ZO-2 upon GSK-3β function, we analyzed the effect of ZO-2 overexpression in two different Wnt reporter constructs in which luciferase expression is driven either by artificial LEF/TCF binding sites or by the Siamois promoter. Overexpression of ZO-2 in

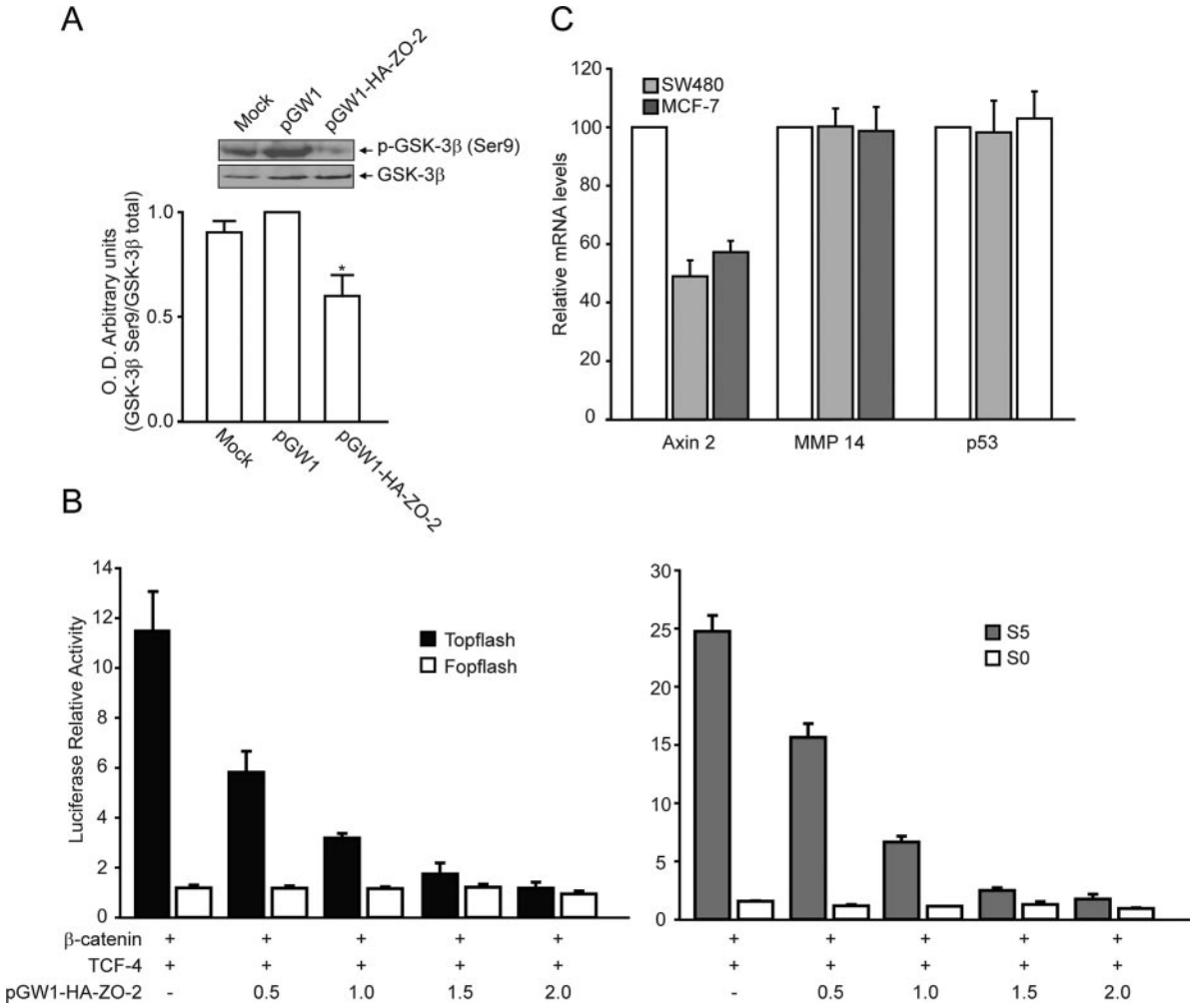

Figure 10. ZO-2 overexpression affects GSK-3β function. (A) The phosphorylation of Ser9 in GSK-3β is diminished upon ZO-2 overexpression. MDCK cells synchronized by serum deprivation for 48 h were transfected with ZO-2 or the empty vector, and after 6 h they were transferred to CDMEM. After 24 h, the cells were lysed and processed for immunoblotting with antibodies against GSK-3β and phosphorylated Ser9 of GSK-3β. (B) ZO-2 represses β-catenin/TCF-4–mediated transcription. HEK293 cells were transiently transfected with β-catenin and hTCF-4 expression plasmids and increasing amounts of a HA-ZO-2 expression vector as indicated. β-Catenin/TCF-4 transcriptional activity was measured by cotransfection of Topflash/Fopflash (left) or Siamois S5/S0 (S5, five TCF-binding sites; S0, all TCF-sites mutated) (right) luciferase reporter gene constructs. (C) ZO-2 specifically represses endogenous *axin-2* but not *MMP14* and *p53* expression in SW480 and MCF-7 cells. SW480 and MCF-7 cells were transiently transfected with 2 μg of pGW1-HA empty vector or pGW1-HA-ZO-2 plasmid. After 12 h, total RNA was isolated to analyze *axin-2*, *MMP14*, and *p53* expression by quantitative RT-PCR by using gene-specific *TaqMan* probes. Expression was normalized to β-actin. Values obtained after transfection with empty vector were set to 100%. Presented data are mean values of four independent experiments.

HEK293 and SW480 cells exhibits a dose-dependent repression of both reporter gene constructs (Figure 10B).

Next, we analyzed by qRT-PCR if the endogenous expression of Wnt target genes Axin-2 and MMP14 is affected by ZO-2 overexpression. Interestingly, in both SW480 and MCF-7 cells, whereas Axin-2 is clearly repressed, matrix metalloproteinase 14 was not repressed (Figure 10C). p53, used as a negative control, was not affected.

ZO-2 Overexpression Promotes CD1 Degradation at the Proteosome

In this context, we next treated MDCK cells transfected with the empty vector or ZO-2, with 50 mM LiCl, because Li^+ has been shown to inhibit GSK-3β activity (Klein and Melton, 1996; Hedgepeth *et al*., 1997). Consistent with our previous results, Li^+ treatment blocked the ZO-2–induced loss of CD1 (Figure 11), confirming the active role of GSK-3β on CD1 degradation. To further study the proteosomal degradation of CD1 triggered by ZO-2, we treated MDCK cells transfected with the empty vector or ZO-2, with the proteosomal inhibitor MG132 (50 μM) and observed an increased amount of CD1 in comparison with untreated cultures (Figure 11). Additionally, we tested whether ZO-2 expression stimulated CD1 degradation at the lysosome. For this purpose, we treated ZO-2–transfected and –untransfected cultures with cloroquine, a weak base that accumulates in lysosomes dissipating their acidic pH (Wibo and Poole, 1974). Cloroquine treatment did not block in a statistically significant manner ZO-2–induced loss of CD1 (Figure 11). Together, these experiments reveal that ZO-2 expression increases CD1 degradation at the proteosome.

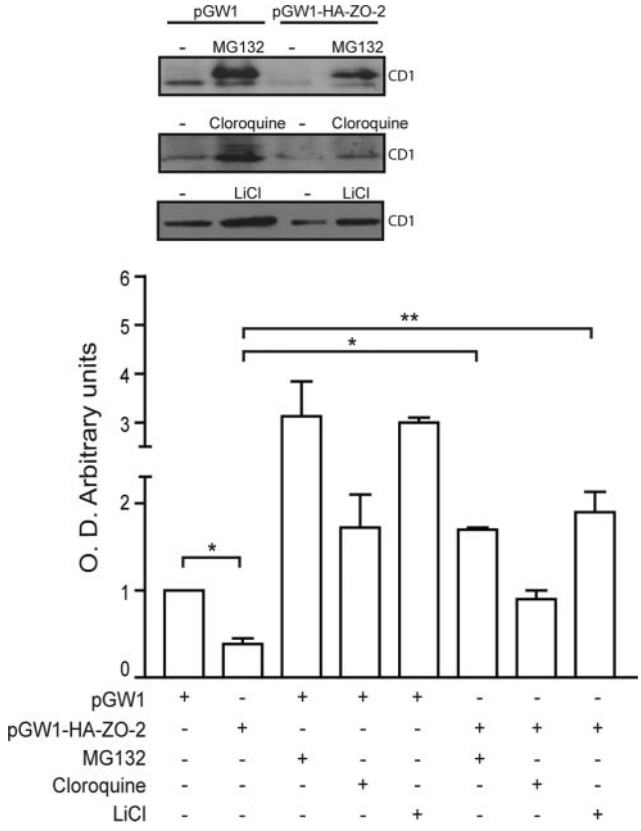

Figure 11. CD1 is degraded at the proteosome upon ZO-2 overexpression. MDCK cells synchronized by serum deprivation for 48 h were next incubated for 24 h in CDMEM and subsequently transfected with ZO-2 or the empty vector. Then, cells were incubated for 24 h in CDMEM. MG132 and chloroquine were added during the last 5 h of incubation with CDMEM, whereas LiCl was included during the last 16 h of incubation. The cells were next lysed and processed for immunoblotting with antibodies against CD1 and actin. For normalization, we gave a value of 1 to the densitometric CD1/actin data, obtained in cells transfected with the empty vector. The mean values ± SE were obtained with the values from three independent experiments. (*$p \leq 0.01$ and **$p \leq 0.001$ according to ANOVA Tukey's multiple comparison test).

DISCUSSION

Although the name ZO-2 indicates that this protein is a TJ protein, the work of us and others demonstrated in recent years that ZO-2 is a dual residency protein found at the nucleus and the cell borders depending on the degree of cell–cell contact (Islas *et al*., 2002; Traweger *et al*., 2003). Because ZO-2 is conspicuously present at the nuclei of sparse epithelial cells, we have become interested in studying the physiological role of nuclear ZO-2 in these cells. Once we found that ZO-2 associated to TFs and down-regulated the activity of reporter genes regulated by promoters under the control of AP-1 sites (Betanzos *et al*., 2004), we started to explore the transcription of which genes is modulated in vivo by ZO-2. Accordingly, we recently showed that the CD1 gene is down-regulated at the transcription level by ZO-2 via an E-box and the TF c-Myc (Huerta *et al*., 2007). Other factors known to repress CD1 transcription are for example the lipid phosphatase PTEN (Chung *et al*., 2006), the tumor suppressor Fhit, (Weiske *et al*., 2007), and the TFs SIP1 (Mejlvang *et al*., 2007) and p53 (Rocha *et al*., 2003).

In this work, we have explored whether ZO-2 overexpression alters the cellular content of CD1 protein. Our results indicate that ZO-2 is able to reduce the protein levels of CD1 in epithelial cells and that this effect is accompanied by a decrease in cell proliferation due to blockade at the G0/G1 phase of the cell cycle, without producing an increase in cellular apoptosis or necrosis.

To our surprise, we were not able to detect any change in the mRNA level triggered by ZO-2 in cells that had been synchronized by serum starvation. These results contrast those previously obtained by us in nonsynchronized cells where the mRNA of CD1 decreases according to the amount of ZO-2 transfected (Huerta *et al*., 2007). To understand this conundrum, we analyzed the mRNA of CD1 present in nonsyncronized and synchronized cells by serum starvation. Our results indicate that serum-deprived cells that are arrested at G0/G1 exhibit a higher level of CD1 mRNA than nonsynchronized proliferating cells. Thus, we suspect that due to the high level of CD1 mRNA found in serum-deprived cells, it is not feasible for ZO-2 to reduce CD1 mRNA in these cells in a significant manner. Interestingly, other studies have revealed cases where CD1 mRNA remains unchanged, whereas CD1 protein content diminishes due to inhibition of translation. For example, 1) in nontransformed intestinal crypt cells, protein kinase C (PKC)α stimulation with phorbol 12-myristate 13-acetate does not affect total CD1 mRNA levels at times when CD1 protein is significantly reduced (Hizli *et al*., 2006). In these cells, activation of PKCα promotes PP2A phosphatase activity that in turn induces the dephosphorylation of the translational repressor 4E-BP1. The hypophosphorylation of 4E-BP1 finally inhibits the translation of CD1 mRNA (Guan *et al*., 2007). 2) The siRNA knockdown of HMGA1, a TF that promotes cell proliferation by accelerating G_1 phase progression, down-

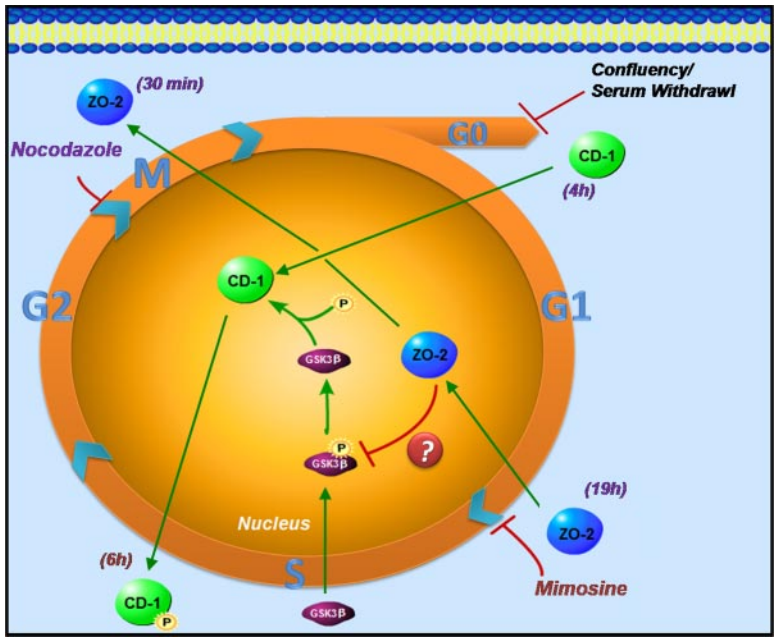

Figure 12. Schematic model depicting the subcellular localization of ZO-2, CD1, and GSK-3β during the cell cycle. At the early stages of G1, CD1 enters the nucleus and initiates cell cycle progression toward the S phase. At the later stages of G1, ZO-2 is imported into the nucleus. GSK-3β enters the nucleus at the S phase, and ZO-2 decreases the inhibitory phosphorylation of GSK-3β at Ser9 by a yet unknown pathway. Activated GSK-3β phosphorylates cyclin D1 at Thr286, triggering CD1 nuclear export, ubiquitination, and degradation by the 26S proteasome. At mitosis, ZO-2 leaves the nucleus and is speculatively recruited to the emerging cell borders of the dividing cells. Time indicated in purple corresponds to time after nocodazole washout, whereas time indicated in brown represents time after mimosine washout.

regulates CD1 protein by translational control involving 4E-BP1 (Kolb *et al*., 2007). 3) The overexpression of PERK, an endoplasmic reticulum transmembrane protein kinase implicated in the mammalian unfolded protein response (UPR) or the activation of UPR with the glycosylation inhibitor tunicamycin, inhibits CD1 synthesis without affecting CD1 mRNA level (Brewer *et al*., 1999; Brewer and Diehl, 2000). PERK blocks CD1 translation by increasing the phosphorylation of the translation elongation initiation factor eIF2α (Brewer and Diehl, 2000) and by augmenting the degradation of CD1 at the proteosome. Apparently, this degradation is dependent upon eIF2α phosphorylation (Raven *et al*., 2008). In a somewhat similar manner, 15-deoxy-$\Delta^{12,14}$-prostaglandin J_2 down-regulates CD1 protein by stimulating eIF2α phosphorylation (Campo *et al*., 2002). 4) A more extreme case is found in rat fibroblasts in which the induced expression of Ras, increases CD1 mRNA level and at the same time decreases CD1 protein synthesis and augments the rate of CD1 degradation at the proteosome (Shao *et al*., 2000).

Here, we have found that ZO-2 transfection accelerates CD1 turnover and promotes CD1 degradation at the proteosome in synchronized cells. In this regard, others have found that retinoic acid that suppresses cell growth at the G1/S cell cycle transition, triggers a decline in CD1 protein, not due to a decreased mRNA expression but to an increased CD1 degradation at the proteosome (Langenfeld *et al*., 1997; Spinella *et al*., 1999). Additionally, the chemotherapeutic agents curcumin, a diferuloylmethane, and GL331, a podophyllotoxin-derived compound, down-regulate the expression of CD1 protein by reducing mRNA expression, inhibiting CD1 promoter-dependent gene expression, and inducing CD1 proteolysis at the proteosome (Lin *et al*., 2001; Mukhopadhyay *et al*., 2002; Srivastava *et al*., 2007).

Because a critical step leading to CD1 degradation involves its phosphorylation at Thr286 by GSK-3β, we studied the impact of ZO-2 overexpression on GSK-3β function. Our results indicate that ZO-2 has a repressive effect not only on an artificial LEF/TCF construct but also on a natural target of the β-catenin signaling pathway, such as Siamois. These results together with our previous observation on the CD1 promoter (Huerta *et al*., 2007) suggest that ZO-2 modulates, in a context-specific manner, the expression of genes involved in cell proliferation and differentiation.

Here, we have also demonstrated that ZO-2 enters the nucleus at the late G1 phase and leaves the nucleus when the cell is in mitosis. This explains why in confluent quiescent cells almost no nuclear ZO-2 staining is detected, whereas in sparse proliferating cells ZO-2 is conspicuously present at the nuclei. The nuclear exit of ZO-2 during mitosis could speculatively occur as a response to the requirement of ZO-2 at the novel plasma membrane established between the dividing cells. With regard to CD1, we found that in MDCK cells the protein enters the nucleus in early G1 and exits the nucleus at the S phase as had been reported previously in fibroblasts (Baldin *et al*., 1993; Diehl *et al*., 1998).

In summary, these results can lead us to propose a model in which ZO-2 enters the nucleus at the late G1 phase, whereas GSK-3β is imported to the nucleus immediately after the G1/S transition (Figure 12). ZO-2, through a yet undefined mechanism, decreases the inhibitory phosphorylation of GSK-3β at Ser9. Activated GSK-3β phosphorylates cyclin D1 at Thr286 triggering CD1 nuclear export and degradation at the proteasome.

ACKNOWLEDGMENTS

We thank the technical help of Victor Hugo Rosales García and Jose de la Luz Diaz Chávez. This work was supported by grant 45691-Q from the Mexican Council for Science and Technology (Consejo Nacional de Ciencia y Tecnologia [CONACYT]). R. T. and M. H. were recipients of doctoral fellowships from CONACYT (166727 and 159492). The work of O. H. was supported by a grant of the Deutsche Forschungsgemeinschaft (FOR721, HU881/4-1).

REFERENCES

Balda, M. S., Garrett, M. D., and Matter, K. (2003). The ZO-1-associated Y-box factor ZONAB regulates epithelial cell proliferation and cell density. J. Cell Biol. *160*, 423–432.

Baldin, V., Lukas, J., Marcote, M. J., Pagano, M., and Draetta, G. (1993). Cyclin D1 is a nuclear protein required for cell cycle progression in G1. Genes Dev. *7*, 812–821.

Betanzos, A., Huerta, M., Lopez-Bayghen, E., Azuara, E., Amerena, J., and Gonzalez-Mariscal, L. (2004). The tight junction protein ZO-2 associates with Jun, Fos and C/EBP transcription factors in epithelial cells. Exp. Cell Res. *292*, 51–66.

Brannon, M., Gomperts, M., Sumoy, L., Moon, R. T., and Kimelman, D. (1997). A beta-catenin/XTcf-3 complex binds to the siamois promoter to regulate dorsal axis specification in *Xenopus*. Genes Dev. *11*, 2359–2370.

Brewer, J. W., and Diehl, J. A. (2000). PERK mediates cell-cycle exit during the mammalian unfolded protein response. Proc. Natl. Acad. Sci. USA *97*, 12625–12630.

Brewer, J. W., Hendershot, L. M., Sherr, C. J., and Diehl, J. A. (1999). Mammalian unfolded protein response inhibits cyclin D1 translation and cell-cycle progression. Proc. Natl. Acad. Sci. USA *96*, 8505–8510.

Brown, E. J., Albers, M. W., Shin, T. B., Ichikawa, K., Keith, C. T., Lane, W. S., and Schreiber, S. L. (1994). A mammalian protein targeted by G1-arresting rapamycin-receptor complex. Nature *369*, 756–758.

Campo, P. A., Das, S., Hsiang, C. H., Bui, T., Samuel, C. E., and Straus, D. S. (2002). Translational regulation of cyclin D1 by 15-deoxy-delta(12,14)-prostaglandin J(2). Cell Growth Differ. *13*, 409–420.

Chlenski, A., Ketels, K. V., Korovaitseva, G. I., Talamonti, M. S., Oyasu, R., and Scarpelli, D. G. (2000). Organization and expression of the human zo-2 gene (tjp-2) in normal and neoplastic tissues. Biochim. Biophys. Acta *1493*, 319–324.

Chlenski, A., Ketels, K. V., Tsao, M. S., Talamonti, M. S., Anderson, M. R., Oyasu, R., and Scarpelli, D. G. (1999). Tight junction protein ZO-2 is differentially expressed in normal pancreatic ducts compared to human pancreatic adenocarcinoma. Int. J. Cancer *82*, 137–144.

Chung, J. H., Ostrowski, M. C., Romigh, T., Minaguchi, T., Waite, K. A., and Eng, C. (2006). The ERK1/2 pathway modulates nuclear PTEN-mediated cell cycle arrest by cyclin D1 transcriptional regulation. Hum. Mol. Genet. *15*, 2553–2559.

Coqueret, O. (2002). Linking cyclins to transcriptional control. Gene *299*, 35–55.

Cross, D. A., Alessi, D. R., Cohen, P., Andjelkovich, M., and Hemmings, B. A. (1995). Inhibition of glycogen synthase kinase-3 by insulin mediated by protein kinase B. Nature *378*, 785–789.

Dasso, M. (1999). Cell Cycle Analysis. In: Current Protocols in Cell Biology, ed. J. Bonifacino, M. Dasso, B. J. Harford, J. Lippincott-Schwartz, and K. M. Yamada, New York: John Wiley & Sons, Inc., 8.0.1–8.4.18.

Dennis, P. B., Jaeschke, A., Saitoh, M., Fowler, B., Kozma, S. C., and Thomas, G. (2001). Mammalian TOR: a homeostatic ATP sensor. Science *294*, 1102–1105.

Diehl, J. A., Cheng, M., Roussel, M. F., and Sherr, C. J. (1998). Glycogen synthase kinase-3beta regulates cyclin D1 proteolysis and subcellular localization. Genes Dev. *12*, 3499–3511.

Fang, Y., Vilella-Bach, M., Bachmann, R., Flanigan, A., and Chen, J. (2001). Phosphatidic acid-mediated mitogenic activation of mTOR signaling. Science *294*, 1942–1945.

Frame, S., and Cohen, P. (2001). GSK3 takes centre stage more than 20 years after its discovery. Biochem. J. *359*, 1–16.

Gingras, A. C., Gygi, S. P., Raught, B., Polakiewicz, R. D., Abraham, R. T., Hoekstra, M. F., Aebersold, R., and Sonenberg, N. (1999). Regulation of 4E-BP1 phosphorylation: a novel two-step mechanism. Genes Dev. *13*, 1422–1437.

Gladden, A. B., and Diehl, J. A. (2005). Location, location, location: the role of cyclin D1 nuclear localization in cancer. J. Cell. Biochem. *96*, 906–913.

Glaunsinger, B. A., Weiss, R. S., Lee, S. S., and Javier, R. (2001). Link of the unique oncogenic properties of adenovirus type 9 E4-ORF1 to a select interaction with the candidate tumor suppressor protein ZO-2. EMBO J. *20*, 5578–5586.

Gonzalez-Mariscal, L., Betanzos, A., and Avila-Flores, A. (2000). MAGUK proteins: structure and role in the tight junction. Semin. Cell Dev. Biol. *11*, 315–324.

Gonzalez-Mariscal, L., Betanzos, A., Nava, P., and Jaramillo, B. E. (2003). Tight junction proteins. Prog. Biophys. Mol. Biol. *81*, 1–44.

Gonzalez-Mariscal, L., Chavez, d. R., and Cereijido, M. (1985). Tight junction formation in cultured epithelial cells (MDCK). J. Membr. Biol. *86*, 113–125.

Gonzalez-Mariscal, L., Lechuga, S., and Garay, E. (2007). Role of tight junctions in cell proliferation and cancer. Prog. Histochem. Cytochem. *42*, 1–57.

Gonzalez-Mariscal, L., Ponce, A., Alarcon, L., and Jaramillo, B. E. (2006). The tight junction protein ZO-2 has several functional nuclear export signals. Exp. Cell Res. *312*, 3323–3335.

Guan, L., Song, K., Pysz, M. A., Curry, K. J., Hizli, A. A., Danielpour, D., Black, A. R., and Black, J. D. (2007). Protein kinase C-mediated down-regulation of cyclin D1 involves activation of the translational repressor 4E-BP1 via a phosphoinositide 3-kinase/Akt-independent, protein phosphatase 2A-dependent mechanism in intestinal epithelial cells. J. Biol. Chem. *282*, 14213–14225.

Gumbiner, B., Lowenkopf, T., and Apatira, D. (1991). Identification of a 160-kDa polypeptide that binds to the tight junction protein ZO-1. Proc. Natl. Acad. Sci. USA *88*, 3460–3464.

Hamilton, B. T., and Snyder, J. A. (1982). Rapid completion of mitosis and cytokinesis in PtK cells following release from nocodazole arrest. Eur. J. Cell Biol. *28*, 190–194.

Hedgepeth, C. M., Conrad, L. J., Zhang, J., Huang, H. C., Lee, V. M., and Klein, P. S. (1997). Activation of the Wnt signaling pathway: a molecular mechanism for lithium action. Dev. Biol. *185*, 82–91.

Hernandez, S., Chavez, M. B., and Gonzalez-Mariscal, L. (2007). ZO-2 silencing in epithelial cells perturbs the gate and fence function of tight junctions and leads to an atypical monolayer architecture. Exp. Cell Res. *313*, 1533–1547.

Hizli, A. A., Black, A. R., Pysz, M. A., and Black, J. D. (2006). Protein kinase C alpha signaling inhibits cyclin D1 translation in intestinal epithelial cells. J. Biol. Chem. *281*, 14596–14603.

Huerta, M., Munoz, R., Tapia, R., Soto-Reyes, E., Ramirez, L., Recillas-Targa, F., Gonzalez-Mariscal, L., and Lopez-Bayghen, E. (2007). Cyclin D1 is transcriptionally down-regulated by ZO-2 via an E box and the transcription factor c-Myc. Mol. Biol. Cell *18*, 4826–4836.

Islas, S., Vega, J., Ponce, L., and Gonzalez-Mariscal, L. (2002). Nuclear localization of the tight junction protein ZO-2 in epithelial cells. Exp. Cell Res. *274*, 138–148.

Jaramillo, B. E., Ponce, A., Moreno, J., Betanzos, A., Huerta, M., Lopez-Bayghen, E., and Gonzalez-Mariscal, L. (2004). Characterization of the tight junction protein ZO-2 localized at the nucleus of epithelial cells. Exp. Cell Res. *297*, 247–258.

Klein, P. S., and Melton, D. A. (1996). A molecular mechanism for the effect of lithium on development. Proc. Natl. Acad. Sci. USA *93*, 8455–8459.

Kolb, S., Fritsch, R., Saur, D., Reichert, M., Schmid, R. M., and Schneider, G. (2007). HMGA1 controls transcription of insulin receptor to regulate cyclin D1 translation in pancreatic cancer cells. Cancer Res. *67*, 4679–4686.

Krude, T. (1999). Mimosine arrests proliferating human cells before onset of DNA replication in a dose-dependent manner. Exp. Cell Res. *247*, 148–159.

Langenfeld, J., Kiyokawa, H., Sekula, D., Boyle, J., and Dmitrovsky, E. (1997). Posttranslational regulation of cyclin D1 by retinoic acid: a chemoprevention mechanism. Proc. Natl. Acad. Sci. USA *94*, 12070–12074.

Latorre, I. J., Roh, M. H., Frese, K. K., Weiss, R. S., Margolis, B., and Javier, R. T. (2005). Viral oncoprotein-induced mislocalization of select PDZ proteins disrupts tight junctions and causes polarity defects in epithelial cells. J. Cell Sci. *118*, 4283–4293.

Lin, S., Huang, H. C., Chen, L. L., Lee, C. C., and Huang, T. S. (2001). GL331 induces down-regulation of cyclin D1 expression via enhanced proteolysis and repressed transcription. Mol. Pharmacol. *60*, 768–775.

Livak, K. J., and Schmittgen, T. D. (2001). Analysis of relative gene expression data using real-time quantitative PCR and the 2(-Delta Delta C(T)) method. Methods *25*, 402–408.

Mejlvang, J., Kriajevska, M., Vandewalle, C., Chernova, T., Sayan, A. E., Berx, G., Mellon, J. K., and Tulchinsky, E. (2007). Direct repression of cyclin D1 by SIP1 attenuates cell cycle progression in cells undergoing an epithelial mesenchymal transition. Mol. Biol. Cell *18*, 4615–4624.

Mukhopadhyay, A., Banerjee, S., Stafford, L. J., Xia, C., Liu, M., and Aggarwal, B. B. (2002). Curcumin-induced suppression of cell proliferation correlates with down-regulation of cyclin D1 expression and CDK4-mediated retinoblastoma protein phosphorylation. Oncogene *21*, 8852–8861.

Nave, B. T., Ouwens, M., Withers, D. J., Alessi, D. R., and Shepherd, P. R. (1999). Mammalian target of rapamycin is a direct target for protein kinase B: identification of a convergence point for opposing effects of insulin and amino-acid deficiency on protein translation. Biochem. J. 344, 427–431.

Nicotera, P., Leist, M., and Ferrando-May, E. (1999). Apoptosis and necrosis: different execution of the same death. Biochem. Soc. Symp. *66*, 69–73.

Peterson, R. T., Beal, P. A., Comb, M. J., and Schreiber, S. L. (2000). FKBP12-rapamycin-associated protein (FRAP) autophosphorylates at serine 2481 under translationally repressive conditions. J. Biol. Chem. *275*, 7416–7423.

Polakiewicz, R. D., Schieferl, S. M., Gingras, A. C., Sonenberg, N., and Comb, M. J. (1998). mu-Opioid receptor activates signaling pathways implicated in cell survival and translational control. J. Biol. Chem. *273*, 23534–23541.

Pullen, N., and Thomas, G. (1997). The modular phosphorylation and activation of p70s6k. FEBS Lett. *410*, 78–82.

Raven, J. F., Baltzis, D., Wang, S., Mounir, Z., Papadakis, A. I., Gao, H. Q., and Koromilas, A. E. (2008). PKR and PKR-like endoplasmic reticulum kinase induce the proteasome-dependent degradation of cyclin D1 via a mechanism requiring eukaryotic initiation factor 2{alpha} phosphorylation. J. Biol. Chem. *283*, 3097–3108.

Rocha, S., Martin, A. M., Meek, D. W., and Perkins, N. D. (2003). p53 represses cyclin D1 transcription through down regulation of Bcl-3 and inducing increased association of the p52 NF-kappaB subunit with histone deacetylase 1. Mol. Cell. Biol. *23*, 4713–4727.

Sabatini, D. M., Erdjument-Bromage, H., Lui, M., Tempst, P., and Snyder, S. H. (1994). RAFT *1*, a mammalian protein that binds to FKBP12 in a rapamycin-dependent fashion and is homologous to yeast TORs. Cell *78*, 35–43.

Sabers, C. J., Martin, M. M., Brunn, G. J., Williams, J. M., Dumont, F. J., Wiederrecht, G., and Abraham, R. T. (1995). Isolation of a protein target of the FKBP12-rapamycin complex in mammalian cells. J. Biol. Chem. *270*, 815–822.

Shao, J., Sheng, H., DuBois, R. N., and Beauchamp, R. D. (2000). Oncogenic Ras-mediated cell growth arrest and apoptosis are associated with increased ubiquitin-dependent cyclin D1 degradation. J. Biol. Chem. *275*, 22916–22924.

Shaulian, E., and Karin, M. (2002). AP-1 as a regulator of cell life and death. Nat. Cell Biol. *4*, E131–E136.

Sourisseau, T., Georgiadis, A., Tsapara, A., Ali, R. R., Pestell, R., Matter, K., and Balda, M. S. (2006). Regulation of PCNA and cyclin D1 expression and epithelial morphogenesis by the ZO-1-regulated transcription factor ZONAB/DbpA. Mol. Cell. Biol. *26*, 2387–2398.

Spinella, M. J., Freemantle, S. J., Sekula, D., Chang, J. H., Christie, A. J., and Dmitrovsky, E. (1999). Retinoic acid promotes ubiquitination and proteolysis of cyclin D1 during induced tumor cell differentiation. J. Biol. Chem. *274*, 22013–22018.

Srivastava, R. K., Chen, Q., Siddiqui, I., Sarva, K., and Shankar, S. (2007). Linkage of curcumin-induced cell cycle arrest and apoptosis by cyclin-dependent kinase inhibitor p21(/WAF1/CIP1). Cell Cycle *6*, 2953–2961.

Tamaoki, T., Nomoto, H., Takahashi, I., Kato, Y., Morimoto, M., and Tomita, F. (1986). Staurosporine, a potent inhibitor of phospholipid/Ca++ dependent protein kinase. Biochem. Biophys. Res. Commun. *135*, 397–402.

Traweger, A., Fuchs, R., Krizbai, I. A., Weiger, T. M., Bauer, H. C., and Bauer, H. (2003). The tight junction protein ZO-2 localizes to the nucleus and interacts with the heterogeneous nuclear ribonucleoprotein scaffold attachment factor-B. J. Biol. Chem. *278*, 2692–2700.

Weiske, J., Albring, K. F., and Huber, O. (2007). The tumor suppressor Fhit acts as a repressor of beta-catenin transcriptional activity. Proc. Natl. Acad. Sci. USA *104*, 20344–20349.

Weiske, J., and Huber, O. (2006). The histidine triad protein Hint1 triggers apoptosis independent of its enzymatic activity. J. Biol. Chem. *281*, 27356–27366.

Wibo, M., and Poole, B. (1974). Protein degradation in cultured cells. II. The uptake of chloroquine by rat fibroblasts and the inhibition of cellular protein degradation and cathepsin B1. J. Cell Biol. *63*, 430–440.

Willott, E., Balda, M. S., Fanning, A. S., Jameson, B., Van Itallie, C., and Anderson, J. M. (1993). The tight junction protein ZO-1 is homologous to the Drosophila discs-large tumor suppressor protein of septate junctions. Proc. Natl. Acad. Sci. USA *90*, 7834–7838.

Woods, D. F., Wu, J. W., and Bryant, P. J. (1997). Localization of proteins to the apico-lateral junctions of *Drosophila* epithelia. Dev. Genet. *20*, 111–118.

Zamorano, A., Mellstrom, B., Vergara, P., Naranjo, J. R., and Segovia, J. (2004). Glial-specific retrovirally mediated gas1 gene expression induces glioma cell apoptosis and inhibits tumor growth in vivo. Neurobiol. Dis. *15*, 483–491.